Charge transport in graphene-based mesoscopic realizations of Sachdev-Ye-Kitaev models

Oguzhan Can,* Emilian M. Nica, and Marcel Franz
Department of Physics and Astronomy and Stewart Blusson Quantum Matter Institute, University of British Columbia, Vancouver, B.C., Canada V6T 1Z1

(Received 27 August 2018; revised manuscript received 15 December 2018; published 14 January 2019)

We consider a recent proposal for a physical realization of the Sachdev-Ye-Kitaev (SYK) model in the zeroth-Landau-level sector of an irregularly shaped graphene flake. We study in detail charge transport signatures of the unique non-Fermi-liquid state of such a quantum dot coupled to noninteracting leads. The properties of this setup depend essentially on the ratio p between the number of transverse modes in the lead M and the number of the fermion degrees of freedom N on the SYK dot. This ratio can be tuned via the magnetic field applied to the dot. Our proposed setup gives access to the nontrivial conformal-invariant regime associated with the SYK model as well as a more conventional Fermi-liquid regime via tuning the field. The dimensionless linear-response conductance acquires distinct $\sqrt{p}$ and $1/\sqrt{p}$ dependencies for the two phases, respectively, in the low-temperature limit, with a universal jump at the transition. We find that corrections scale linearly and quadratically in either temperature or frequency on the two sides of the transition. In the weak-tunneling regime, we find differential conductance proportional to the inverse square root of the applied voltage bias U. This dependence is replaced by a conventional Ohmic behavior with constant conductance proportional to $1/\sqrt{T}$ for bias energy eU smaller than temperature scale k_BT. We also describe the out-of-equilibrium current-bias characteristics and discuss various crossovers between the limiting behaviors mentioned above.

DOI: 10.1103/PhysRevB.99.045419

I. INTRODUCTION

Sachdev-Ye-Kitaev (SYK) is an exactly solvable quantum mechanical model describing N fermions with random all-to-all interactions [1,2]. The model is connected to black hole physics in AdS_2 space-time gravity theories through holographic principle [3,4]. It exhibits a host of remarkable properties such as nonvanishing residual entropy [5] and saturating the universal chaos bound [6] which are also properties of quantum black holes. SYK and its variants [7–19] are important examples of holographic quantum matter where non-Fermi-liquid (NFL) behavior is observed in the presence of strong correlations and strong disorder. In a non-Fermi liquid, elementary excitations of the system can not be associated with noninteracting electronic excitations through adiabatic continuity arguments. This means that the familiar quasiparticle description fails, making theoretical considerations difficult. Nevertheless, the SYK model is special: despite the strong correlations, it can be solved in the large-N limit and many observable quantities can be analytically obtained.

The distinct non-Fermi-liquid behavior of the SYK model remains to be experimentally observed. Recently, various realizations of the model have been proposed (see Ref. [20] for a recent review) involving ultracold atoms [21], Majorana modes on the surface of a topological insulator [22], semiconductor quantum wires attached to a quantum dot [23], and finally a graphene flake in external magnetic field [24] which will be the focus in this paper. Remarkably, this relatively simple setup contains all of the essential ingredients of the SYK model. More specifically, the low-energy sector of this system involves electrons in the zeroth Landau level with virtually no kinetic energy. For the chemical potential μ in the zeroth Landau level, the irregular boundary of the flake ensures that the electronic wave functions acquire a random spatial structure. A quasidegeneracy is maintained via the preserved chiral symmetry. Correspondingly, the Coulomb interactions projected onto the lowest Landau level reflect the disorder and are likewise random and all-to-all, as required by the SYK model.

In this paper, we study the tunneling conductance and current-voltage characteristics of a disordered graphene-flake realization [24] of the complex-fermion version of the SYK model [3] in a setup shown in Fig. 1. The transport properties are obtained via analytical and numerical solutions in the limit of large degeneracy of ballistic channels in the leads and of the zeroth Landau level on the graphene-flake quantum dot. Our aim is to provide clear signatures of the nontrivial, conformal-invariant regime of the SYK model which can be readily observed in a charge transport experiment.

Our setup Fig. 1 is reminiscent of well-known quantum-impurity systems, such as the multichannel Kondo model [25]. Although the analogy is not exact, it is natural to expect that the low-temperature properties of the junction are essentially controlled by the ratio of the number of channels in the leads to the effective degeneracy on the dot $p = M/N$. While M is typically fixed by the lead geometry, N can be tuned in our setup via the applied magnetic field on the dot. Therefore, our proposed setup naturally allows for quantum phase transitions as a function of the magnetic field on the graphene flake. Our results, presented below, are in agreement with these expectations.

*Corresponding author: ocan@phas.ubc.ca

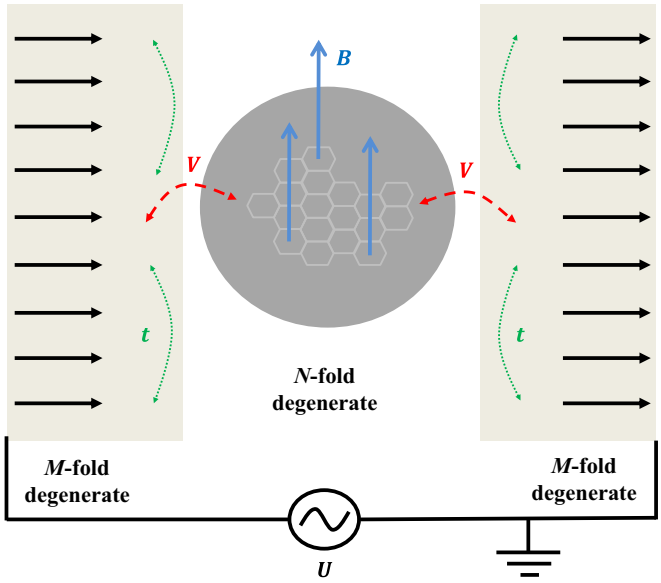

FIG. 1. Sketch of the proposed experimental setup for measurements of tunneling conductance of a graphene-based SYK_4 model. A graphene dot with an irregular boundary is placed under a perpendicular magnetic field B. The Coulomb interactions projected onto the zeroth Landau level of degeneracy N provide an effective realization of an SYK_4 model [24]. The dot is coupled to identical, quasi-one-dimensional, ballistic leads each with M transverse modes. We consider general models which also allow for the effects of disorder on leads in the vicinity of the junction (t). In addition to the random, all-to-all interactions on the dot, which are specific to SYK_4 models, we also include disordered, all-to-all scattering between dot and lead end points V. The applied bias is labeled by U.

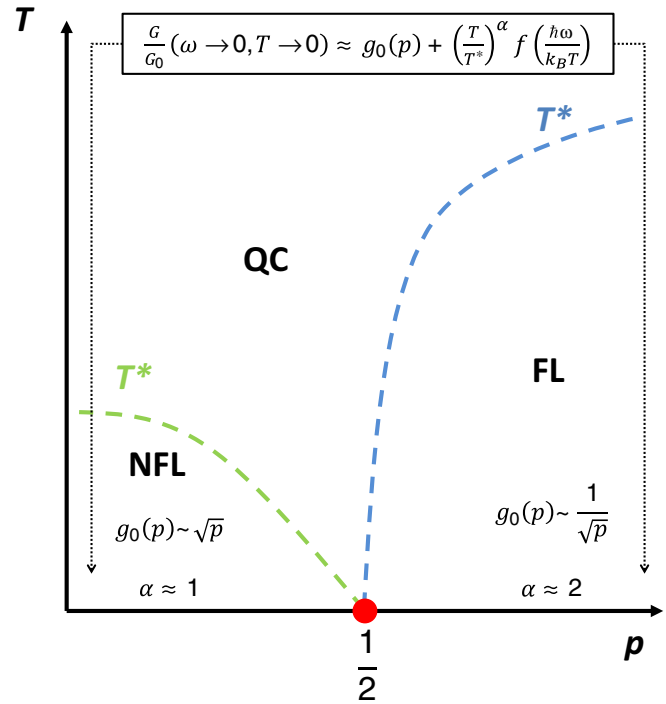

FIG. 2. Sketch of the expected T-p phase diagram of the graphene dot in contact with leads corresponding to the setup in Fig. 1. $p = M/N$ is the ratio between the number of transverse channels in each lead M and the degeneracy of the zeroth Landau level on the dot N, as defined in Eqs. (9)–(11). For fixed M, N and p can be tuned via the applied magnetic field B. At $T = 0$, a second-order quantum phase transition separates an emergent, conformal-invariant NFL regime from a more conventional FL phase, as originally discussed in Ref. [11]. We expect that both regimes survive for finite temperatures below the crossover scales labeled by T^*. The two phases are separated via a quantum-critical (QC) regime, which is not discussed in this work.

Our model for the junction is very similar to the model introduced by Banerjee and Altman (BA) in Ref. [11]. The BA model consists of N fermions described by the SYK_4 Hamiltonian [Eq. (3) below] coupled to M "peripheral" fermions described by an SYK_2 model. Here, SYK_q refers to an SYK model with q-fermion interactions. Because for large enough M the coupling to peripheral noninteracting fermions is a relevant perturbation the BA model exhibits a second-order quantum phase transition at $p = 1$ from an SYK-like NFL phase at small p to a Fermi liquid at large p. In our setup, peripheral fermions describe electrons in the leads. In analogy to the BA results, coupling to the leads can destabilize the SYK state on the dot which makes the transport properties of the junction highly nontrivial.

Our results are summarized in Fig. 2. For subcritical fields ($p < p_c = \frac{1}{2}$), a phase with emergent conformal invariance is realized on the dot well below a crossover scale [11] $\hbar\omega^*(p) \propto k_B T^*$. This regime is characterized by a leading spectral density for the dot electrons which exhibits nontrivial $\omega^{-1/2}$ and $T^{-1/2}$ scaling, as predicted for SYK_4 model in the absence of the leads [3]. Following BA [11], we refer to this as the non-Fermi-liquid phase. Upon approaching the transition, we expect the crossover scale T^* to vanish [11] as $\sqrt{p_c - p}$. For fields above the critical value ($p > p_c$), the effects of the random interactions on the graphene flake become subleading at low temperatures. At frequencies and temperatures below $T^*(p)$, the spectral density of the dot develops a resonance peak with corrections which scale as ω^2 and T^2, as in conventional Fermi-liquid (FL) regimes. The crossover scale T^* is expected to decay to zero as $(p - p_c)$ as we approach the transition from this side [11].

In the particle-hole symmetric case at $T = 0$, we find that the linear-response dimensionless dc tunneling conductance [Eq. (13) below] has a distinct dependence on parameter p:

$$g_0 = \begin{cases} \pi\sqrt{p}, & p < p_c \\ 2/\sqrt{p}, & p > p_c. \end{cases} \tag{1}$$

At the transition, g_0 undergoes a *universal jump* from $\pi/\sqrt{2}$ to $2\sqrt{2}$. At nonzero temperatures, the sharp transition with increasing p is broadened into a smooth crossover. We find corrections to the dimensionless conductance which scale linearly and quadratically with either temperature or frequency on the NFL and FL sides, respectively. Crossovers to quantum-critical and high-temperature regimes are observed with increasing temperature.

In the weak-tunneling regime on the NFL side (i.e., when the dot-lead coupling is the smallest energy scale) we predict

the tunneling differential conductance of the form

$$g(U) \propto \begin{cases} 1/\sqrt{U}, & eU \gg k_B T, \\ 1/\sqrt{T}, & eU \ll k_B T. \end{cases} \tag{2}$$

At low temperature T compared to the applied bias eU the behavior is highly non-Ohmic reflecting the divergent spectral density of the SYK dot at low energy. At higher temperature, the divergence is cut off and a more conventional Ohmic dependence prevails albeit with a highly unusual temperature dependence.

Aside from the linear-response and weak-tunneling regimes, we consider also fully nonequilibrium situations with no natural small parameter in which one can perturb. In this case, we employ the Keldysh formulation of the transport theory. We match these results to the simple limiting cases mentioned above and obtain interesting crossover behaviors as a function of temperature, voltage bias, and lead-dot coupling. Throughout, we focus on the tunneling conductance deep within each of the two stable phases and do not address the behavior in the quantum-critical regime in great detail.

We note that Ref. [26] discussed charge transport in a similar setup involving an irregular graphene flake in the presence of an applied field. The authors consider the limit of few tunneling channels corresponding to $M \to 0$ in our terminology. In the conformal regime for the dot, they find a "duality" in the zero-temperature differential conductance which scales as the square root and inverse of the square root of the bias in the limit of small and large biases, respectively. These results are in effect complementary to those found for our setup, which are valid in the limit of large degeneracy of both leads and dot.

In Section II we describe our model. Section III presents our main results for the frequency- and temperature-dependent conductance obtained in the linear-response regime and the I-V characteristics for arbitrary static biases. Our conclusions are presented in Sec. IV. Detailed discussions of the theory and calculations are available in the Appendices.

II. MODEL

We now describe the setup shown in Fig. 1 in greater detail. As previously mentioned, it consists of an irregularly shaped graphene flake, under a perpendicular magnetic field, in proximity to the end points of two leads each with M quasi-one-dimensional, ballistic modes. We consider leads which are sufficiently long such that effects due to coupling to large reservoirs can be ignored. The low-energy sector of the graphene flake is described by the effectively random interactions within the zeroth-Landau-level manifold of degeneracy N. For a detailed discussion on the realization of the SYK model in the zeroth-LL sector of the irregularly shaped graphene flake, we refer the reader to Ref. [24].

Due to the disorder inherent to the irregularly shaped graphene flake, we expect that the matrix elements for tunneling to and from the end points of the leads are essentially random. We expect that our predictions are valid for systems where both the number of transverse modes M and the degeneracy of the zeroth Landau level N are large, which in practice means at least of $O(10)$. We also assume that the filling of the system can be tuned via applied gate voltages. In this work, we only consider statistically identical left and right leads, with equivalent random hoppings to the dot. In addition, the leads remain in thermal equilibrium with large reservoirs. In the following, we shall refer to the graphene flake and the random disordered end points of the left and right leads as the dot and the leads for simplicity. Note that we ignore the electron spins as the external magnetic field on the dot results in large spin splitting, allowing us to consider only one spin sector [24].

We first consider a setup where the lead end points in the vicinity of the junction are modeled by an *effective local* SYK_2 model, implying that the low-energy dynamics of the lead end point is dominated by disorder scattering. This amounts to ignoring the effects of coupling to the bulk of the *noninteracting leads* to leading order. Equivalently, the neglected couplings are assumed to be marginal or irrelevant in the renormalization group (RG) sense. We stress that this approximation is not an essential part of our model and we show that the two phases and the respective conductances are essentially unchanged when the local disorder on the leads is neglected altogether in favor of a coupling to noninteracting extended leads more typical of quantum-impurity models [27].

The situation described above is modeled by the BA-type Hamiltonian [11] with two flavors of peripheral fermions corresponding to the two leads:

$$H_I = H_D + H_L + H_R + H_{LD} + H_{RD}. \tag{3}$$

The dot is described by the SYK_4 Hamiltonian

$$H_D = \frac{1}{(2N)^{3/2}} \sum_{ijkl} J_{ij;kl} c_i^\dagger c_j^\dagger c_k c_l - \mu \sum_i c_i^\dagger c_i, \tag{4}$$

where $i \in \{1, \ldots, N\}$ labels the degenerate, randomized zeroth-Landau-level states. In the absence of any symmetry, we use the indices i, j, k, l to label four distinct fermions in the zeroth Landau level (LL). As discussed in Ref. [24], the effective vertices $J_{ij;kl}$ are computed by projecting the Coulomb interaction onto the zeroth-LL sector. They result from the spatial average of the spatially random zeroth-LL wave functions of the four electrons. Consequently, they are also randomized in the second-quantized form used here. The antisymmetrized vertex $J_{ij;kl} = -J_{ji;kl} = -J_{ij;lk}$ obeys a Gaussian distribution with zero mean and $\overline{|J_{ij;kl}|^2} = J^2$ variance. Based on the previous proposal [24] for a realization of the SYK_4 model, it is estimated that $J \approx 25$ meV in this setup. We refer the reader to Ref. [24] for an in-depth discussion of the emergence of the SYK model shown in Eq. (4) in the zeroth-LL sector of an irregularly shaped graphene flake under an applied magnetic field.

The end points of the two leads are modeled by a pair of SYK_2 Hamiltonians

$$H_a = \sum_{\alpha\beta} \frac{t_{a,\alpha\beta}}{M^{1/2}} \psi_{a\alpha}^\dagger \psi_{a\beta} + \text{H.c.} - \mu \sum_\alpha \psi_{a\alpha}^\dagger \psi_{a\alpha}, \tag{5}$$

with $a = L, R$ labeling the left and the right lead, respectively. The index $\alpha \in \{1, \ldots, M\}$ corresponds to transverse channels in the bulk of the lead. We assume that the local couplings are drawn from a Gaussian random distribution with zero mean and variance $\overline{|t_{\alpha\beta}|^2} = t^2$. The $1/(2N)^{3/2}$ and $1/\sqrt{M}$ factors

are chosen so that the Hamiltonians exhibit sensible scaling in the thermodynamic limit. Coupling between the dot and the leads is effected by

$$H_{aD} = \sum_{i\alpha} \frac{V_{ai\alpha}}{(NM)^{1/4}} c_i^\dagger \psi_{a\alpha} + \text{H.c.}, \tag{6}$$

where the tunneling matrix elements $V_{a\alpha i}$ are chosen as random Gaussian with $\overline{|V_{a\alpha i}|^2} = V^2$ variance.

Except for two flavors of peripheral fermions $\psi_{a\beta}$ corresponding to two leads H_I is essentially the BA Hamiltonian of Ref. [11] and we may thus adopt results of that work with only minimal modifications. Specifically, we will make an extensive use of the expressions derived by BA for the fermion propagators in the FL and NFL phases. These will be reviewed below as needed. Here, we record for future use the expression for the crossover temperature indicated in Fig. 2,

$$T^*(p) \simeq \begin{cases} (V^4/t^2 J)\sqrt{p_c - p}/p, & p < p_c \\ (V^2/t)\sqrt{p(p - p_c)}, & p > p_c \end{cases} \tag{7}$$

derived in Ref. [11] for p close to p_c.

In a realistic experimental setup, the leads will be spatially extended which we model by connecting the lead end points to semi-infinite ballistic chains for each transverse channel α. This is represented by an "extended lead" Hamiltonian $H^{\text{ext}} = H_I + H_E$ with

$$H_E = \sum_{|\tilde{i}|>1,\alpha} [t_E \psi_{\tilde{i}\alpha}^\dagger \psi_{\tilde{i}+1,\alpha} + \text{H.c.}] - \mu \sum_{|\tilde{i}|>1,\alpha} \psi_{\tilde{i}\alpha}^\dagger \psi_{\tilde{i}\alpha} + \sum_\alpha [t_{-1,\alpha} \psi_{-1\alpha}^\dagger \psi_{L\alpha} + t_{1,\alpha} \psi_{1\alpha}^\dagger \psi_{R\alpha} + \text{H.c.}]. \tag{8}$$

Electrons in the bulk of the leads are annihilated by $\psi_{\tilde{i}\alpha}$, $|\tilde{i}| \geqslant 1$ and are not subject to either disorder or interactions. $t_{1/-1,\alpha}$ are the couplings between the bulk and end-point states. To conserve the large-M degeneracy, we approximate these to be independent of the index α and ignore any randomness. Likewise, we assume that the M transverse channels in the bulk are quasidegenerate on a scale set by the variance of the interactions on the dot J. Throughout, we ignore any source of asymmetry between left and right leads. In our calculations, we set $t_{1/-1} > t = V = J/2 > 0$ unless otherwise stated.

In considering an effective local model for the junction, we ignore the coupling to the bulk of the leads which are given by $H_{EL/R}$. As previously mentioned and supported by numerical results in Sec. III, including these terms and/or ignoring any local disorder on the lead end points does not modify our main results.

We estimate the degeneracy of the zeroth LLs N (from Ref. [24]) and the number of quasi-one-dimensional, ballistic modes in each lead M in our setup as

$$N = \frac{SB}{\Phi_0}, \tag{9}$$

$$M = \frac{hG_L}{e^2}, \tag{10}$$

where S is the area of the graphene flake, B is the applied field, and $\Phi_0 = hc/e$ is the quantum of flux. M is related to the conductance of the extended ballistic leads G_L. We also define the auxiliary quantities $p = M/N$, $G_0 = (e^2/2h)\sqrt{MN}$, and $\tilde{G}$ which can be estimated from

$$p(B) = \frac{hG_L\Phi_0}{e^2 SB}, \tag{11}$$

$$G_0(B) = \sqrt{\frac{e^2 G_L SB}{4h\Phi_0}}, \tag{12}$$

$$\tilde{G}(\omega, T, B) = \frac{G(\omega, T, B)}{G_0(B)}, \tag{13}$$

where $G(\omega, T, B)$ is the conductance of the junction. As previously mentioned, with M fixed, the ratio p can be tuned via the strength of the transverse field applied to the dot. Note that both G_0 and p are functions of the applied field.

III. CHARGE TRANSPORT

The model defined by Hamiltonian H_I in Eq. (3) can be solved analytically using path-integral techniques to average over disorder in the limit of large N and M. Specifically, closed form expressions for fermion propagators can be obtained [11] in the conformal regime $(\omega, T) \ll J$. From these, it is possible to evaluate the conductance of the junction in certain limits, including the linear-response regime (small-bias voltage U) and the weak-tunneling regime (small V). This leads to our main results already given in the Introduction as Eqs. (1) and (2).

Away from these simple limits and outside the conformal regime we solve the model in Eq. (3) numerically using a large-(N, M) saddle-point approximation and determine the real-time Green's functions in the Keldysh basis [17] in and out of equilibrium. In practice, this amounts to numerically iterating a set of self-consistent equations, given in Appendix B 1, for the fermion propagators and self-energies. Based on these solutions, we obtain the response to an applied bias using a variant of the standard Meier-Wingreen formula [28]. The numerical results are restricted to finite temperatures and are matched to the analytical results in appropriate limits. A detailed discussion of our calculations is given in the Appendices.

A. Linear-response ac conductance

We first discuss the tunneling conductance obtained via the Kubo formalism [29] in the presence of a small oscillating bias applied to the two leads and subsequently present our results for current with arbitrarily large, static biases. A detailed account of our calculations is found in Appendix A.

Based on dimensional analysis [30], we expect that the dimensionless conductance of the junction [Eq. (13)] obeys the scaling form

$$\frac{G}{G_0} = g\left(\frac{\hbar\omega}{k_B T}, \frac{T}{T^*}, \frac{\mu}{\mu^*}, p\right), \tag{14}$$

where g is a dimensionless function which depends on the nature of the phases on either side of the transition. In addition, ω is the frequency of the driving bias, T is the temperature, μ is the chemical potential common to both leads and dot, while $p \propto \frac{1}{B}$ serves as a tuning parameter. $T^*(p)$ is given in Eq. (7) and represents crossover scales associated with the

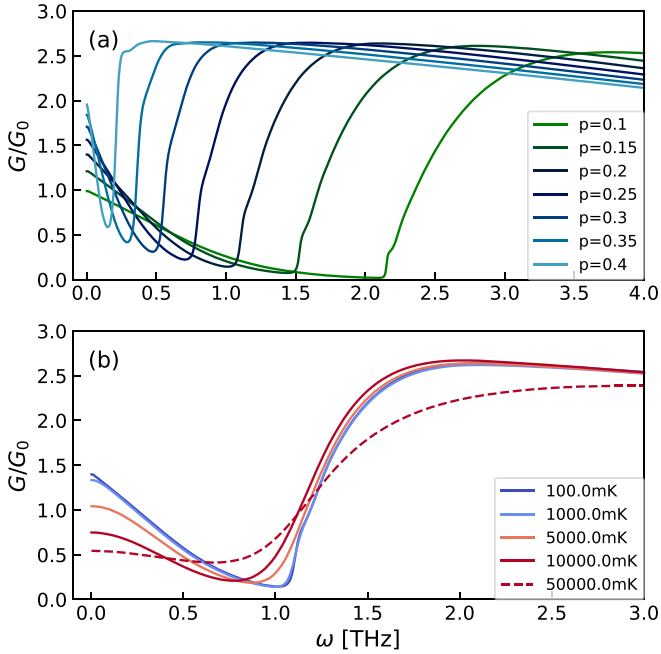

FIG. 3. (a) Dimensionless tunneling conductance computed using Eq. (A15) and numerical solutions of the saddle-point equations in the NFL regime at fixed temperature $T = 100$ mK and increasing values of the tuning parameter p [Eq. (11)]. Note the crossover from the peak at low energies, in the conformal-invariant NFL regime, to the broad, featureless spectrum beyond a scale $\hbar\omega^* \approx k_B T^*$. With increasing p, ω^* decreases, while the peak is suppressed. The behavior is consistent with the approach to a second-order quantum phase transition as sketched in Fig. 2. (b) Same as (a), at fixed $p = 0.2$ and for several temperatures. The height of the peak at lower frequencies decreases with increasing temperature indicating a smooth crossover away from the conformal-invariant NFL regime. Also note the crossover to the high-frequency limit which occurs at roughly the same frequency. The dashed line corresponds to the high-temperature limit and is included for comparison.

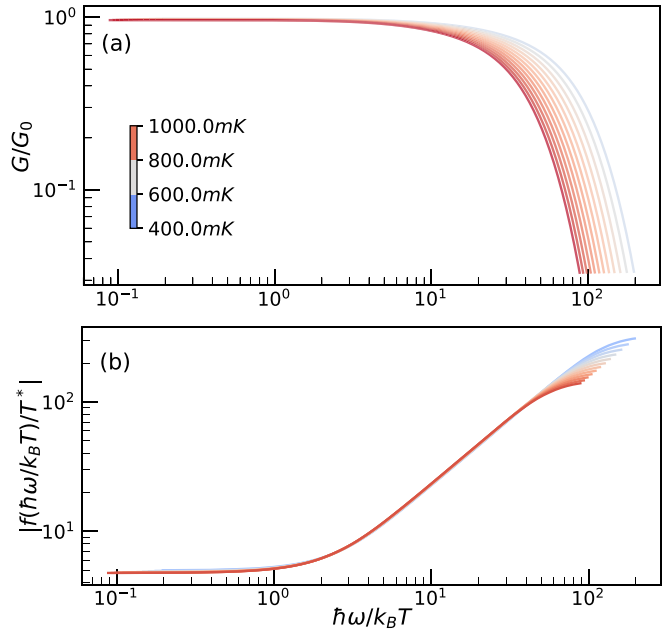

FIG. 4. (a) Dimensionless tunneling conductance [Eq. (A15)] in the NFL regime for $p = 0.1$ as a function of $\hbar\omega/k_B T$ for several temperatures. The conductances saturate close to a universal value $g_0(p)$ [Eq. (15)] for vanishing values of the argument. Deviations are clearly visible for arguments roughly exceeding 1. (b) Scaling collapse for the function f which determines the corrections to the universal dimensionless conductance $g_0(p)$ in the conformal-invariant regime [Eq. (15)]. It scales linearly for arguments greater than $O(1)$.

emergence of the NFL and FL scaling regimes. It vanishes at the critical point from either side. As Ref. [11] pointed out, away from particle-hole symmetry ($\mu \neq 0$), the NFL and FL phases are separated by an incompressible phase for a finite range of μ. Since the focus of our work is behavior of the conductance deep within either NFL and FL phases, we do not address the intermediate phases. As such, we associate $\mu^*(p)$ with a scale below and above which the conductance follows either NFL/FL scaling. As discussed below, for frequencies and temperatures well below T^*, the conductance shows very weak dependence on either ω, T, while it exhibits characteristic scaling with $p(B)$ in either phase.

In Fig. 3(a), we plot the dimensionless tunneling conductance G/G_0 as a function of frequency at combined half-filling $\mu = 0$ and at a temperature of 100 mK in the NFL regime for increasing values of the tuning parameter $p < p_c = \frac{1}{2}$. Here and below, we take $J = 25$ meV as estimated for the graphene flake in Ref. [24]. In addition, we assume $t = V = J/2$ in the following unless otherwise noted. We distinguish the presence of a relatively sharp peak in the conformal-invariant NFL regime at low frequencies followed by a crossover to an essentially featureless spectrum beyond a scale $\omega^*(p)$. Upon increasing p, the height of the peak increases while the crossover scale tends to zero, as expected for a second-order quantum phase transition (Fig. 2). In Fig. 3(b) we plot the conductance at fixed $p = 0.2$ on the NFL side for several temperatures. With decreasing T, the height of the central peak increases while its width remains roughly constant. The broad spectrum beyond the crossover scale shows very little dependence on temperature.

The dimensionless conductance $G/G_0(B)$ at half-filling is shown in Fig. 4(a) as a function of $\hbar\omega/k_B T$, for $p = 0.1$, and temperatures ranging from 400 to 1000 mK. It saturates to a constant for values of the argument below 1. A weak temperature dependence in this limit can still be distinguished from the offsets of the saturated values. These shifts are due to corrections from leading irrelevant operators about the conformal-invariant fixed-point value which arise with increasing temperature. We find that in the $\hbar\omega, k_B T \ll k_B T^*$ limit the dimensionless conductance is consistent with the scaling form

$$g\left(\frac{\hbar\omega}{k_B T}, \frac{T}{T^*} \to 0, 0, p\right) = g_0(p) - \left(\frac{T}{T^*}\right)^{\alpha} f\left(\frac{\hbar\omega}{k_B T}\right). \tag{15}$$

The universal dimensionless conductance $g_0(p)$ is the contribution in the conformal limit. It varies continuously along the line of fixed points associated with the stable NFL phases. We estimated $\alpha \approx 1$ for a range of temperatures extending over a decade from the lowest numerically accessible value

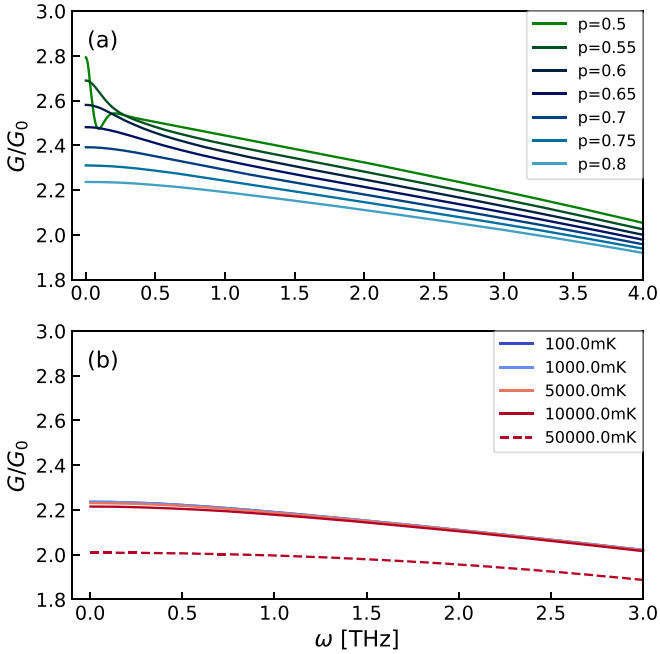

FIG. 5. (a) Dimensionless tunneling conductance [Eq. (A15)] in the FL regime at fixed temperature $T = 100$ mK and increasing values of the tuning parameter p. The peak around zero frequencies rapidly broadens and merges with the featureless spectrum at higher frequencies. (b) Same as (a), at fixed $p = 0.8$ and for several temperatures. Note the insensibility to variations in temperature relative to the NFL regime [Fig. 3(b)]. The dashed line corresponds to the high-temperature limit and is included for comparison.

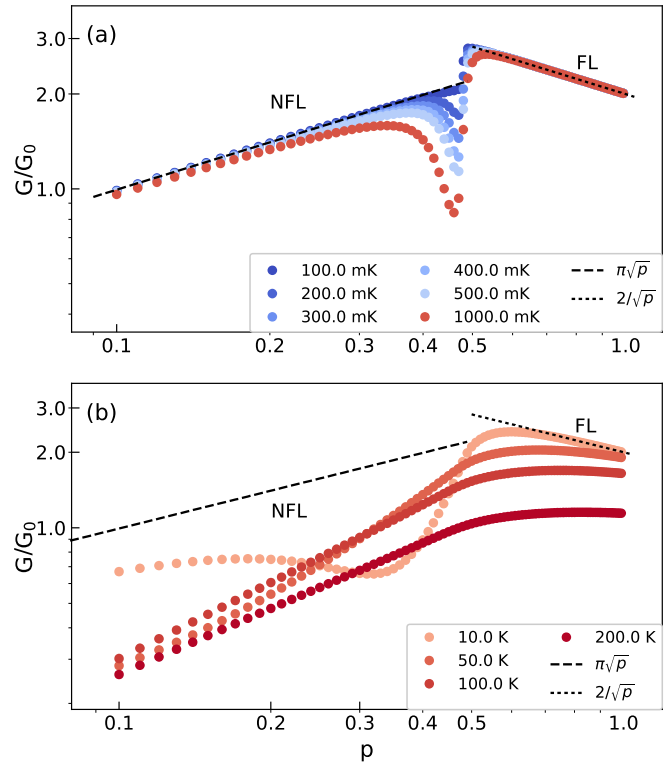

FIG. 6. Dimensionless dc conductance G/G_0 as function of tuning parameter p, for a range of temperatures, at particle-hole symmetry, plotted on a logarithmic scale. The dashed and dotted gray lines denote the analytically determined, universal conductances $g_0(p)$ given in Eq. (1). The full dots are the numerically extracted dc conductances obtained by taking the $\omega \to 0$ limits of ac conductances computed using Eq. (A15). (a) When T is below $T^*(p)$ for almost all values of p, the numerical results in each phase are in good agreement with the analytical prediction for $g_0(p)$. Deviations are more pronounced with increasing temperatures, especially on the NFL side, reflecting corrections due to the finite crossover scale $T^*(p)$. (b) For temperatures exceeding $T^*(p)$ in the entire range of p values, we observe a crossover to a putative quantum-critical regime on the NFL side, as illustrated by the $T = 10$ K curve. As the temperature is further increased, we note the onset of a high-temperature regime as indicated by the remaining curves.

of 100 mK (see Appendix A 3). The exponent also holds for higher values of p. In Fig. 4(b), we plot the universal function f which converges to a constant for small values of $\hbar\omega/k_BT$. For higher values of the argument, f scales linearly. This indicates that corrections to the conductance about the conformal-invariant NFL fixed point scale linearly with either frequency or temperature. Similar behavior emerges for other values of p, as well as in cases away from particle-hole symmetry. We note that the temperature- and frequency-dependent corrections to the universal dimensionless conductance g_0 arise from the subleading contributions to the leading spectral densities shown in Eqs. (A17) and (A18) and Fig. 15.

Turning to the FL regime, in Fig. 5(a) we plot the dimensionless conductance G/G_0 as a function of frequency, at half-filling, for fixed temperature $T = 100$ mK and several values of p. Close to the transition, we observe a narrow peak which quickly broadens and flattens and becomes indistinguishable from the high-energy spectrum. In addition, as shown in Fig. 5(b), it shows a much weaker temperature dependence relative to the NFL phase in Fig. 3(b). An analysis similar to the one leading to Eq. (15) reveals a similar scaling form with an exponent $\alpha = 2$ which is characteristic of FL regimes [31] (see Appendix A 3). The relative insensibility to temperature on the FL side is most likely due to the combined effect of corrections to the fixed point which scale as $(T/T^*)^2$ and to a relatively large crossover scale, as sketched in Fig. 2. A similar picture emerges in this regime away from particle-hole symmetry.

B. Linear-response dc conductance

We now discuss the universal dimensionless conductance $g_0(p)$ defined in Eq. (15) and compare our analytical and numerical results. Well below the crossover scales determined by $T^*(p)$, $g_0(p)$ provides the leading contribution to the dimensionless conductance G/G_0. Appendix A 2 gives analytical calculation of $g_0(p)$ in the dc ($\omega = 0$) and zero-temperature limits. The linear-response dc conductance is then given via the spectral densities for the coupled leads and dot in the conformal regime. At particle-hole symmetry, a simple result already quoted in Eq. (1) is obtained using BA results for the spectral densities (adapted to two flavors of auxiliary fermions). It shows a universal jump at $p = p_c$.

At nonzero temperature, the integrals entering the Kubo formula must be evaluated numerically. Our results for G/G_0 are shown in Fig. 6(a) as a function of p, at several lower temperatures, in the $\mu = 0$ case. On the NFL side ($p < p_c$) we

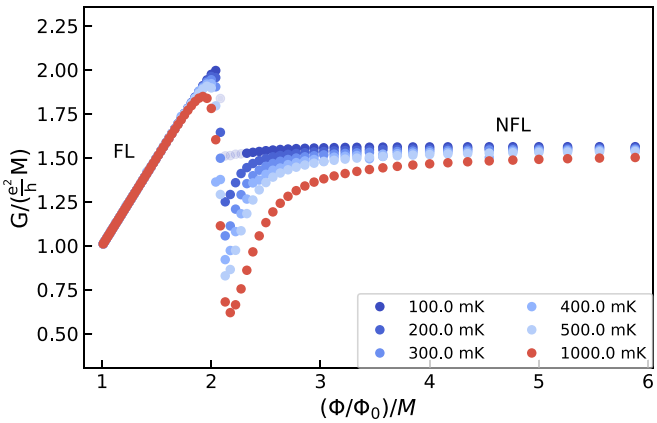

FIG. 7. Dimensionless tunneling conductance per lead channel as a function of flux threading the dot. Note that $\frac{(\Phi/\Phi_0)}{M} = 1/p$ [see also Eq. (11)]. The conductance shows linear dependence for low values of external magnetic field in the FL phase below the critical point. With increasing field, the sharp crossover to the NFL behavior is observed. In the latter regime, the dimensionless conductance is constant in the applied field.

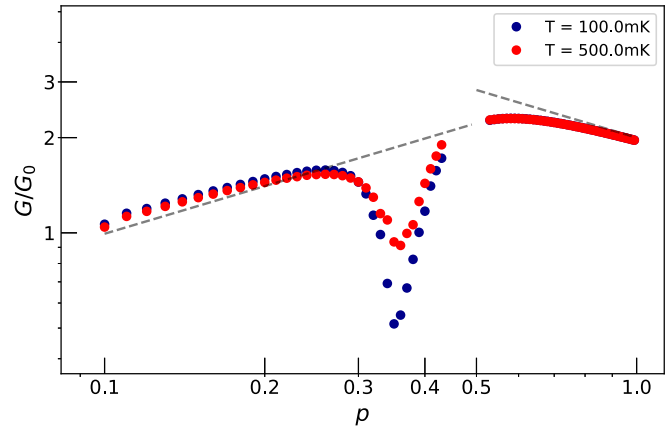

FIG. 8. Dimensionless tunneling conductance at $T = 100$ and 500 mK in the dc limit, away from half-filling ($\mu = 0.625$ meV). The dashed lines indicate the behavior at particle-hole symmetry. The curves closely follow the particle-hole symmetric dependence on $\sqrt{p}$ on the NFL side. On the FL side, we observe stronger deviations in the vicinity of the crossover, although the $1/\sqrt{p}$ behavior is recovered for $p > 1$.

find that the numerically determined dc conductance closely follows the analytical prediction for $g_0(p)$, provided that T stays well below $T^*(p)$. We attribute the large deviations observed above roughly 500 mK to proximity to the quantum-critical regime. Similarly, crossovers to the quantum-critical regime with increasing p are more pronounced and occur at lower values with increasing temperature. This behavior is completely consistent with the presence of a crossover scale $T^*(p)$ which vanishes continuously at the critical coupling, as sketched in Fig. 2. It is also in agreement with the offsets of the saturated values in Fig. 4.

Beyond the crossover to the quantum-critical regime, the dc conductance enters the FL phase, where it exhibits very little dependence on temperature. With increasing temperatures, we find that the dimensionless conductance G/G_0 exhibits several crossovers. To illustrate, in Fig. 6(b) we plot the dimensionless conductance G/G_0 as a function of p for temperatures exceeding 1 K. Note the crossover to a putative quantum-critical regime for $p < \frac{1}{2}$, as illustrated by the $T = 10$ K data. The remaining curves indicate the onset of a distinct, high-temperature regime. We also note that a distinction between the NFL and FL regimes survives in this high-temperature regime.

In order to illustrate the direct dependence of the response on the applied external magnetic field to the dot, we include Fig. 7, which shows the dimensionless conductance per transverse channel as a function of the flux threading the dot. The linear increase in the FL regime reflects the increasing number of channels available for conduction in the dot which is linearly proportional to the Landau-level degeneracy N. Above the transition, which occurs at total magnetic flux $\Phi = 2M\Phi_0$, conductance saturates at a field-independent constant value $\frac{\pi}{2}\frac{e^2}{h}M$ characteristic of the NFL regime. Observing this remarkable behavior experimentally would constitute an unambiguous evidence of the SYK physics in the system.

Away from exact half-filling, the dc conductance can still be evaluated analytically. In the conformal limit on the NFL side we obtain (Appendix A 2)

$$g_0(p < 1/2) = \pi \sin\left(\frac{\pi}{2} + 2\theta\right)\sqrt{p}. \tag{16}$$

The phase $\theta \in [-\pi/4, \pi/4]$ is related to the "spectral asymmetry" defined in the context of SYK$_4$ models [3,11,25]. As discussed in Ref. [11], it is in general a function of the total filling of dot and lead (end points) and of $p = M/N$. For particle-hole symmetry, $\theta = 0$ for all values of p. Away from particle-hole symmetry, θ must be determined numerically. In Fig. 8, we show the dc conductance for a chemical potential $\mu = 0.625$ meV ($0.025J$) and at two temperatures as a function of tuning parameter p. The dashed line indicates the expected value at particle-hole symmetry extracted via Eq. (1). In the NFL regime, the dimensionless conductance closely follows the particle-hole symmetric results and shows similar scaling with p. The total filling at $p = 0$ is 0.42 and undergoes a 10% increase up to close to the transition. Larger deviations of the conductance with respect to the particle-hole symmetric case are observed in the FL regime for $p \gtrsim \frac{1}{2}$, although the curve approaches the scaling predicted for the particle-hole symmetric case for $p > 1$. In this regime, the total filling varies from 0.46 to 0.48 at $p = 1$. As mentioned above, we do not treat the crossover regimes in great detail in this work. The results indicate that small departures from particle-hole symmetry do not significantly affect the $\sqrt{p}$ scaling determined for $\mu = 0$.

C. Nonlinear dc response

We also calculated the nonlinear current (C9) for arbitrary *static* applied bias across the dot via an approach based on real-time Green's functions in the Keldysh basis [28,32]. The leads are in thermal equilibrium with reservoirs at chemical potentials shifted by $\pm eU/2$, where U is the applied bias. The details of the procedure and implementation are given in Appendix C. In Fig. 9 we plot the current in arbitrary units,

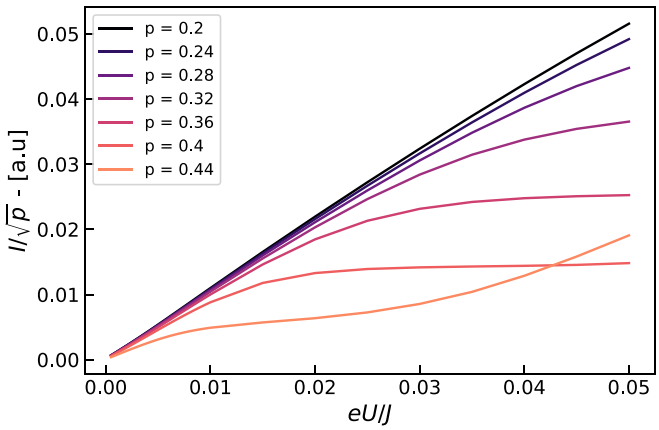

FIG. 9. Tunneling current [Eq. (C9)] in arbitrary units scaled by $\sqrt{p}$, at a fixed temperature $T = 400$ mK $(2.0 \times 10^{-4} J)$ for the leads, for several values of the tuning parameters $p < p_c$ corresponding to the NFL near equilibrium, as a function of bias eU in units of J. A crossover from linear response can be distinguished around $U^*(p)$.

scaled with $\sqrt{p}$ as a function of the applied bias in units of J, at a lead temperature of $T = 400$ mK $(2.0 \times 10^{-4} J)$, for a range of values of the tuning parameter p, corresponding to the NFL in equilibrium. The factor of $\sqrt{p}$ is included to account for variations with tuning parameter already present in linear response. The response remains linear up to a bias $U^*(p)$ beyond which it saturates to a p-dependent constant. The crossover scale set by the bias $eU^*(p)$ decreases and appears to vanish as p approaches the value at which the transition occurs in equilibrium $p_c = \frac{1}{2}$. We note that this behavior persists for applied biases which are well above the scale set by the temperature in equilibrium. In Fig. 10 we show the current, likewise in arbitrary units, at fixed $T = 400$ mK for the leads, for a range of applied biases eU, as a function of tuning parameter p. The dashed line indicates the current predicted from linear response at the same temperature. For vanishingly small biases, the current closely follows the linear-response prediction with characteristic $\sqrt{p}$ and $1/\sqrt{p}$ scaling in the NFL and FL regimes, respectively. Within an expected shift reflecting the linear dependence on bias, the scaling behavior persists for p away from $p_c = \frac{1}{2}$ up to biases of $O(10^{-2})J$, while the crossover region becomes increasingly broader. Beyond this hallmark bias, the currents for $p < p_c$ undergo a clear crossover to an intermediate regime which is no longer well described by a $\sqrt{p}$ dependence. Finally, for large biases approaching J, a completely different p dependence is reached, which still maintains a distinction between the two regimes encountered in linear response. There is a striking similarity between the crossovers observed in the nonlinear response with increasing bias and the crossovers seen with increasing temperatures in linear response [Figs. 6(a) and 6(b)] as a function of p.

The numerical saddle-point results are consistent with a lead-dot coupling which is relevant in the RG sense. Hence, we expect that the results for the conductance discussed thus far, which imply renormalized spectral densities for the leads (Appendix B 3), are always valid in the $T \ll T^*(p)$ limit. Note that according to Eq. (7) the crossover scale T^* is expected [11] to be of $O(V^4/t^2 J)$ in the lead-dot coupling V.

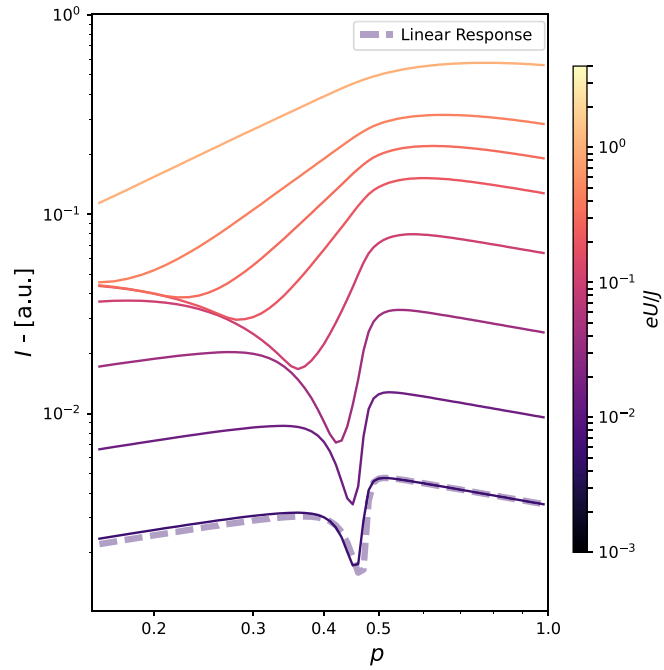

FIG. 10. Tunneling current [Eq. (C9)] in arbitrary units, at fixed $T = 400$ mK $(2.0 \times 10^{-4} J)$ for the leads, for a range of biases eU across the dot, as a function of tuning parameter p. The results are plotted on a logarithmic scale. The dashed line indicates the prediction based on linear response. For biases up to $O(10^{-2} J)$, the current closely follows the $\sqrt{p}$ and $1/\sqrt{p}$ dependencies encountered in linear response, up to a trivial shift due to near-linear dependence of the current on bias. Increasing bias induces a crossover to an intermediate regime $O(10^{-1}) < eU/J < O(1)$ analogous to the quantum-critical region near equilibrium. Note the similarity with the temperature-induced crossovers in Figs. 6(a) and 6(b).

For a weak coupling between leads and dot, the crossovers determined by T^* are expected to occur at very low temperatures. Above T^*, we can estimate the current-bias curve using a weak-tunneling approximation discussed below.

D. Weak-tunneling regime

When the coupling between leads and the dot V is sufficiently small, one can calculate the tunneling current perturbatively in this small parameter even when the bias voltage across the two leads is finite. This amounts to the well-known tunneling Hamiltonian approximation [29] involving a tunneling rate of $O(V^2)$ and densities of states corresponding to decoupled leads and SYK_4 dot in the conformal-invariant regime. More specifically, we expect that this regime emerges for temperatures well above the crossover scale T^*. Below this scale, the contribution from V is nonperturbative, as illustrated by the spectral densities calculated to all orders in V in Eqs. (A17) and (A18) and Fig. 15. Since we expect that $T^* \propto V^4$ [Eq. (7)] in the vicinity of the transition, a reduction in V will induce a significant decrease in T^*. We found that the weak-tunneling current I_{WT} is given by

$$\langle I_{\mathrm{WT}} \rangle \propto \begin{cases} eU/\sqrt{T} & (eU \ll k_B T), \\ \sqrt{eU} & (eU \gg k_B T). \end{cases} \tag{17}$$

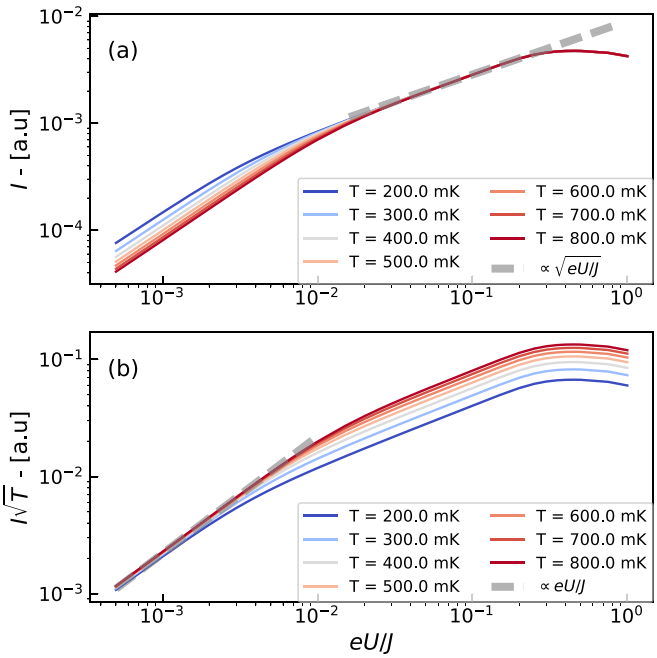

FIG. 11. Current in weak-tunneling approximation for the NFL phase, plotted in arbitrary units as a function of applied bias eU in units of J. Here, we take $t = J/2$, $V = 0.025J$, and $p = 0.3$. (a) In high-bias regime $eU \gg k_B T$ we find that the current calculated with (C9) using numerical solutions of the saddle-point equations match weak-tunneling analytical prediction (17) plotted with dashed lines. (b) $I\sqrt{T}$-eU/J characteristics in the weak-tunneling regime for various temperatures. For low-bias regime $eU \ll k_B T$ we observe a scaling collapse, confirming the predicted $eU/\sqrt{T}$ dependence.

Details of the calculation are presented in Appendix D. The weak-tunneling approximation is expected to be valid in the context of scanning tunneling spectroscopy (STM) experiments and in situations when leads are separated from the dot by a thin oxide barrier.

We match these analytical predictions to the nonlinear current (C9) which includes contributions to all orders in V. To tune the system to the weak-coupling regime, we use a lead-dot coupling $V = 0.025J$ which is one order of magnitude smaller than the previously used value while all remaining parameters, including the temperature range, are kept fixed. The numerically determined current for $p = 0.3$, at various temperatures ranging from $T = 200$ to 800 mK, as a function of applied bias eU is shown in Fig. 11. In high-bias regime [Fig. 11(a)] where $eU \gg k_B T$ the I-V curves do not depend on temperature and agree with the analytical prediction $I \propto \sqrt{eU/J}$. At low biases, we observe a temperature-dependent behavior which is linear in the applied bias. In Fig. 11(b) we plot $I\sqrt{T}$ versus eU to observe the scaling collapse that occurs for $I \propto eU/\sqrt{T}$ in low-bias regime ($eU \ll k_B T$). Once again, this characteristic behavior, if observed experimentally, would furnish strong evidence supporting the SYK state on the dot.

E. Effect of extended leads

Our results thus far have neglected the effect of the coupling to the bulk of the leads on the low-energy and low-temperature spectral densities. Instead, we considered an *effective local model* for the junction where disorder scattering dominated the low-energy dynamics of the end points of the leads. We now consider an explicit coupling to extended leads as described by Hamiltonian (8). A detailed discussion of the modified saddle-point solution is given in Appendix E.

We find that including a coupling to noninteracting extended leads or ignoring disorder scattering altogether near the end points has no essential effect on the low-temperature tunneling current in either phase. Consider the effect of coupling to extended leads, which are modeled as quasi-one-dimensional, ballistic wires, while maintaining the disorder

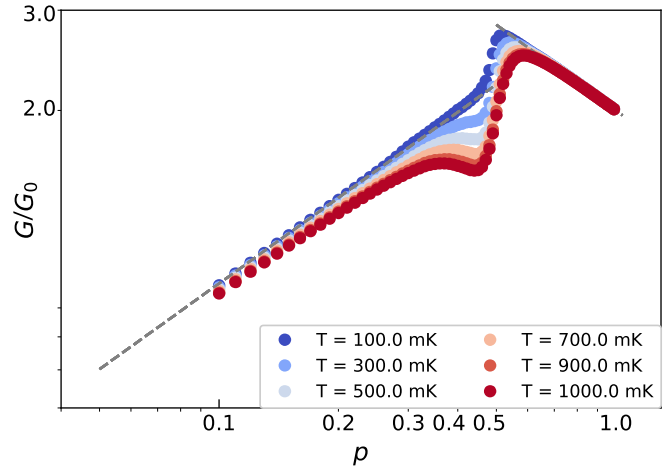

FIG. 12. Dimensionless conductance for an effective model of the tunneling junction which includes strong coupling of $O(J/2)$ to extended, noninteracting leads (see Appendix E) in addition to the local disorder on the lead end points, plotted versus tuning parameter p. The same essential features present in Fig. 6(a) for the effective model without local contributions from the lead bulk are also apparent here. The main difference is a narrowing of the crossover regime.

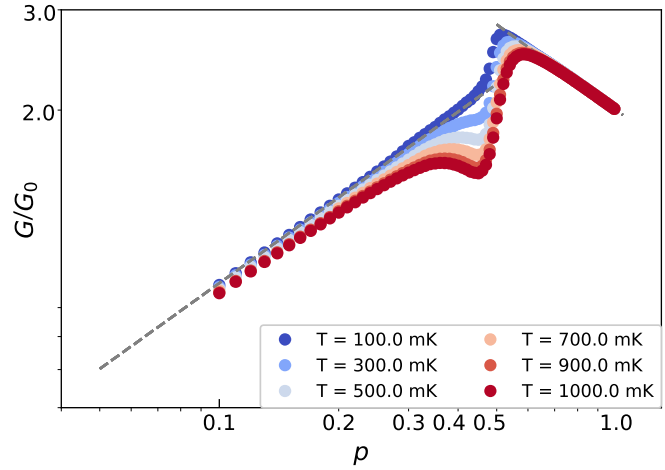

FIG. 13. Dimensionless conductance for an effective model which includes strong coupling to extended, noninteracting leads of $O(J/2)$ but excludes any local disorder on the lead end points. As in Fig. 12, we observe no essential deviations from the cases shown Fig. 6.

at the end points. At weak coupling, such additional terms are marginal. A complete numerical solution indicates that both phases survive for couplings to the bulk of the leads of order J. Likewise, a transition to the FL occurs at the same value of p_c. The dc conductance preserves the same scaling with p in either phase, as shown in Fig. 12(a) for $\mu = 0$. A similar picture emerges upon completely neglecting the disorder in the end points of the leads, as shown in Fig. 13. We thus conclude that the simplified model of the junction studied in the earlier subsections constitutes a very reasonable approximation for a physical setup with extended leads.

IV. SUMMARY AND CONCLUSIONS

We have characterized the tunneling conductance and current-bias properties of a graphene quantum-dot realization of the SYK model coupled to leads with and without disorder in the vicinity of the junction. The problem is highly nontrivial because the fragile non-Fermi-liquid state on the dot is easily disrupted by coupling to the leads. We obtained our results using a saddle-point approximation for an effective model of the junction in the limit of large number of transverse modes M for the lead and large degeneracy of the dot zeroth Landau level N, with their ratio $p = M/N$ finite. The calculations were carried out analytically in various simple limits and numerically using real-time Green's functions in the Keldysh basis for general parameters. We find clear signatures of distinct emergent conformal-invariant non-Fermi-liquid and Fermi-liquid regimes and of the crossovers associated with a quantum-critical point. The transition can be accessed by tuning the ratio p via the magnetic field applied to the dot.

Deep within the NFL phase, and for temperatures much lower than a crossover scale T^*, we find a universal dimensionless conductance which shows a $\sqrt{p}$ variation with the tuning parameter which is directly related to the applied field B through Eq. (11). This dependence is intrinsic to the low-energy emergent, conformal-invariant regime. We also find leading corrections which scale linearly with temperature and frequency throughout the NFL regime. Beyond the transition at $p_c = \frac{1}{2}$, we find that the low-temperature FL regime exhibits a $1/\sqrt{p}$ dependence on the tuning parameter and corrections which are quadratic in either temperature or frequency. Results obtained at weak particle-hole asymmetry show a similar scaling with tuning parameter p.

We find that the current is linear with applied bias up to a bias $U^*(p)$ when the coupling to the leads is strong. For larger biases we find crossovers from the linear to intermediate- and high-bias regimes which are analogous to the quantum-critical and high-temperature regions in linear response.

In the limit of weak tunneling, relevant for scanning tunneling spectroscopy and tunnel junction experiments, we find the tunneling conductance proportional to $\min(1/\sqrt{U}, 1/\sqrt{T})$. The inverse square-root dependence on the bias in the $T \to 0$ limit reflects the $|\omega|^{-1/2}$ behavior of the electron spectral function in the NFL regime of the SYK model and has been noted previously [24,26]. Our calculations extend these results to include the effect of nonzero temperature which is found to cut off the low-bias divergence of the conductance at a characteristic value proportional to $1/\sqrt{T}$. We also find that the similar scaling with p holds in the absence of local disorder on the lead end points.

We note that our results are in some ways similar to those obtained for $\mathrm{SU}(K) \otimes \mathrm{SU}(N)$ multichannel Kondo impurity models where K and N refer to the number of conduction electron channels and spin-symmetry group, respectively [25]. These models host nontrivial emergent conformal invariance at low temperatures and are amenable to saddle-point approximations. It was found that the conduction electron scattering rate depends essentially on the ratio between K and N. Corrections at finite temperature or frequency scale with a common nontrivial fixed-point-dependent exponent [25,33]. In our case, we find that the conductance in the NFL phase acquires an analogous $\sqrt{p}$ dependence. However, we find corrections which scale linearly with temperature and frequency throughout the NFL phase for all ratios $p < p_c$.

A closely related aspect involves the small-bias corrections to the differential tunneling conductance (Fig. 9). In the context of two-channel Kondo models, corrections which exhibit eU/k_BT scaling for $eU, k_BT \ll T_K$ have been predicted based on conformal field theory [34,35], and nonequilibrium Green's functions calculations [36,37]. These corrections scale as x^2 and $\sqrt{x}$, for $x \ll 1$ and $x \gg 1$, respectively, where $x = eU/k_BT$. These predictions were subsequently observed in experiment [38]. Based on the analogy with the two-channel Kondo model, and the linear scaling with temperature in equilibrium, we expect a differential conductance with corrections which are linear in the bias, for $k_BT \ll eU \ll k_BT^*$ in our case. Equivalently, we expect corrections to the Ohmic dependence which are quadratic in the bias in this regime. Our results shown in Fig. 9 do not show any signatures of this behavior as the current exhibits a linear dependence on bias up to a crossover scale eU^* which is roughly analogous to k_BT^* in equilibrium. Here, we argue that this is likely due the smallness of these corrections which are expected to be $\sim (eU)^2/T^* \approx O(10^{-3})J$. We reserve a more detailed analysis of this issue for future work.

As these results indicate, the SYK model realized in a graphene flake or a similar system shows a remarkable wealth of experimentally observable transport phenomena when connected to weakly interacting leads. Perhaps the most important finding is that the strength of coupling to the leads is less important than the total number of channels present in the leads ($2M$ in our notation with two identical leads). When $2M$ exceeds the number N of the active fermion degrees of freedom on the SYK dot a quantum phase transition is triggered to a Fermi-liquid state. Much of the interesting SYK phenomenology is then lost (although some signatures may remain in the quantum-critical regime at higher temperatures or frequencies). This result, already contained in the work of Banerjee and Altman [11], underscores the necessity of designing the junction with a small number of conduction channels coupled to the dot. STM tip normally corresponds to a single-channel probe, which would be ideal to observe properties deep in the NFL regime. It is important to remember, however, that a sample in the STM experiment must be grounded and, according to our results, coupling to the ground must be carefully controlled so that the *total* number of channels coupled to the dot remains small compared to N.

Because N is equal to the number of magnetic flux quanta piercing the dot, the sensitive dependence on the parameter $p = M/N$ affords a unique opportunity to study the quantum phase transition from NFL to FL phase by tuning the applied field. At low temperature, we predict a universal jump in dimensionless dc conductance at the transition accompanied by a characteristic broadening at nonzero T. Observing such a jump would constitute an unambiguous evidence of the phase transition as well as the SYK state on the high-field side of the transition.

We may thus conclude that transport experiments on a nanoscale graphene flake with an irregular boundary offer a unique opportunity to study the iconic SYK model, whose physics cuts across the boundaries of fields ranging from string theory and quantum gravity to chaos theory and strongly correlated electron systems.

ACKNOWLEDGMENTS

We thank I. Affleck, J. Folk, É. Lantagne-Hurtubise, and C. Li for stimulating discussions. Research reported in this paper was financially supported by NSERC and CIfAR. Final stages of the work were completed at the Aspen Center for Physics (M.F.). O.C. was also financially supported by QuEST program at the Stewart Blusson Quantum Matter Institute, UBC.

APPENDIX A: LINEAR RESPONSE

1. Tunneling conductance in the saddle-point approximation

We calculate the tunneling current as a function of applied oscillating potentials on the lead (end points) included via the terms

$$H \to H + H_{U,L} + H_{U,R}, \tag{A1}$$

$$H_{U,L/R} = \pm\left(\frac{eU}{2}\right)\cos(\omega_0 t)\sum_{\alpha}\psi^{\dagger}_{\alpha,L/R}\psi_{\alpha,L/R}, \tag{A2}$$

where U is the amplitude of the scalar potential and H is the Hamiltonian for the junction [Eq. (3)].

We eliminate the scalar potential via a temporal gauge transformation which introduces time-dependent phases (Sec. 3.4 of Ref. [39])

$$\phi(t) = \left(\frac{eU}{2\hbar}\right)\frac{\sin(\omega_0 t)}{\omega_0}, \tag{A3}$$

$$\hbar\frac{d\phi}{dt} = \left(\frac{eU}{2}\right)\cos(\omega_0 t). \tag{A4}$$

This amounts to the gauge transformation $H_{U,R/L} \to 0$ and

$$H_{L/RD} \to H_{LR/D}(t) = \sum_{i\alpha}\frac{V_{i\alpha}}{(NM)^{1/4}}c_i^{\dagger}\psi_{L/R\alpha}e^{\mp i\phi(t)} + \sum_{i\alpha}\frac{V^{*}_{i\alpha}}{(NM)^{1/4}}\psi^{\dagger}_{L/R\alpha}e^{\pm i\phi(t)}c_i. \tag{A5}$$

We remind the reader that the tunneling coefficients $V_{L,R}$ connecting left/right lead and dot are chosen to be complex, random, Gaussian-distributed variables of identical variance V^2. As such, we suppress L/R indices. We expand the coupling between left/right lead and dot to linear order in the phase

$$\begin{aligned} H_{L/RD}(t) \approx & \sum_{i\alpha}\frac{V_{i\alpha}}{(NM)^{1/4}}c_i^{\dagger}\psi_{L/R\alpha} + \sum_{i\alpha}\frac{V^{*}_{i\alpha}}{(NM)^{1/4}}\psi^{\dagger}_{L/R\alpha}c_i \\ & \mp i\frac{eU\sin(\omega_0 t)}{2\hbar\omega_0}\sum_{i\alpha}\frac{V_{i\alpha}}{(NM)^{1/4}}c_i^{\dagger}\psi_{L/R\alpha} \\ & \pm i\frac{eU\sin(\omega_0 t)}{2\hbar\omega_0}\sum_{i\alpha}\frac{V^{*}_{i\alpha}}{(NM)^{1/4}}\psi^{\dagger}_{L/R\alpha}c_i \\ = & H_{L/RD}(U=0) \pm A(t) I_{L/RD}. \end{aligned} \tag{A6}$$

The currents *out of left and right leads* are obtained from $\langle I_{L/R}\rangle = (ie/\hbar)\langle[N_{L/R}, H]\rangle$

$$\langle I_{L/R}\rangle = \frac{ie}{\hbar}\sum_{i,\alpha}\left\{\frac{V_{Li\alpha}}{(NM)^{1/4}}\langle\psi^{\dagger}_{L\alpha}c_i\rangle - \frac{V^{*}_{Li\alpha}}{(NM)^{1/4}}\langle c_i^{\dagger}\psi_{L\alpha}\rangle\right\}, \tag{A7}$$

where $N_{L/R}$ is the total number operator for left and right leads, respectively, and

$$A(t) = \frac{U\sin(\omega_0 t)}{2\omega_0}. \tag{A8}$$

Following the standard linear-response formalism [40], the current is

$$\overline{\langle I_{L/R}(t)\rangle} = \int_{-\infty}^{\infty} dt' A(t') C^{R}(t-t'), \tag{A9}$$

where we defined the disorder-averaged, retarded current-current correlator

$$C^{R}(t-t') = -i\theta(t-t')\overline{\langle[I_{L/R}(t), I_{L/R}(t')]\rangle}. \tag{A10}$$

After a Fourier transform, we obtain

$$\overline{\langle I_{L/R}(t)\rangle} = \frac{\mathrm{Im}C^{R}(\omega_0)}{\omega_0}\left(\pm\frac{U}{2}\cos(\omega_0 t)\right) - i\frac{\mathrm{Re}C^{R}(\omega_0)}{\omega_0}\left(\pm\frac{U}{2}\sin(\omega_0 t)\right), \tag{A11}$$

where $\mathrm{Im}C^{R}$ and $\mathrm{Re}C^{R}$ are odd and even functions, respectively.

We identify the tunneling conductance

$$G(\omega, T, \mu, p) = \frac{\mathrm{Im}C^R(\omega)}{2\omega}. \tag{A12}$$

Note the additional factor of $\frac{1}{2}$. Recall that we assume symmetric leads implying equal conductance for the left and right junctions. Furthermore, U is the total potential difference between the two leads, as opposed to $U/2$ across each left/right junction. The factor of $\frac{1}{2}$ then yields the conductance of the entire system.

The retarded, disorder-averaged, current-current correlator C^R can be determined by considering its imaginary-time-ordered analog:

$$C^T(\tau - \tau') = \frac{e^2}{\hbar^2 (NM)^{1/4}} \sum_{i,j,\alpha,\beta} \left\{ \overline{V_{i\alpha} V^*_{j\beta} \langle T \psi^\dagger_\alpha(\tau) c_i(\tau) c^\dagger_j(\tau') \psi_\beta(\tau') \rangle} + \overline{V^*_{i\alpha} V_{j\beta} \langle T c^\dagger_i(\tau) \psi_\alpha(\tau) \psi^\dagger_\beta(\tau') c_j(\tau') \rangle} \right\} \tag{A13}$$

$$= \frac{-e^2 V^2 \sqrt{NM}}{\hbar^2} \{ G_c(\tau - \tau') G_\psi(\tau' - \tau) + G_\psi(\tau - \tau') G_c(\tau' - \tau) \}, \tag{A14}$$

where the bar indicates disorder averaging. We also temporarily suppressed L/R indices for clarity. In obtaining the last line, we used the fact that at saddle point the lead and dot electrons are decoupled [11] with single-particle Green's functions G_c and G_ψ which are diagonal in the α and i indices. Taking into account the definition of V [Eq. (3)], the summation over the indices produces the overall factor of $\sqrt{NM}$.

Straightforward Fourier transform, change to the Lehmann representation, Matsubara frequency summation [29], and subsequent analytical continuation lead to the expression for the tunneling conductance

$$G(\omega, T, \mu, p) = \frac{e^2 V^2 \sqrt{NM} \pi}{2\hbar} \left\{ \int_{-\infty}^{\infty} d\epsilon \, \rho_c(\epsilon, T) \rho_\psi(\epsilon + \omega, T) \left[\frac{f(\epsilon) - f(\epsilon + \omega)}{\omega} \right] + (\psi \leftrightarrow c) \right\}, \tag{A15}$$

where we introduced the spectral densities $\rho_{c,\psi}(\omega, T) = -(1/\pi)\mathrm{Im}G_{c,\psi}(\omega, T)$, and the standard Fermi-Dirac function $f(\omega)$. We also suppressed the explicit dependence of the spectral densities on μ and p for simplicity.

2. Direct current and zero-temperature limits

In the dc limit the conductance is given by

$$\lim_{\omega \to 0} G = \frac{e^2 V^2 \sqrt{NM} \pi}{2 k_B T} \int_{-\infty}^{\infty} d\epsilon \, \rho_c(\epsilon, T) \rho_\psi(\epsilon, T) \left(\frac{1}{\cosh^2 \left(\frac{\hbar \epsilon}{4 k_B T} \right)} \right). \tag{A16}$$

In the emergent conformal-invariant regime on the NFL side, $\hbar\omega, k_B T \ll k_B T^*$, we approximate the spectral densities by the forms given in Appendix A of Ref. [11]:

$$\rho_c(\epsilon, T) = \frac{B_c}{J} \left(\frac{k_B T}{J} \right)^{-1/2} \frac{e^{-\alpha/2}}{\sqrt{2}\pi^2} \cosh \left(\frac{\hbar \epsilon}{2 k_B T} \right) \frac{\Gamma\left(\frac{1}{4} - i \frac{\alpha}{2\pi} + i \frac{\hbar \epsilon}{\pi 2 k_B T} \right) \Gamma\left(\frac{1}{4} + i \frac{\alpha}{2\pi} - i \frac{\hbar \epsilon}{\pi 2 k_B T} \right)}{\Gamma\left(\frac{1}{2} \right)}, \tag{A17}$$

$$\rho_\psi(\epsilon) = \frac{B_\psi}{J} \left(\frac{k_B T}{J} \right)^{1/2} \frac{e^{-\alpha/2} \sqrt{2}}{\pi^2} \cosh \left(\frac{\hbar \epsilon}{2 k_B T} \right) \frac{\Gamma\left(\frac{3}{4} - i \frac{\alpha}{2\pi} + i \frac{\hbar \epsilon}{\pi 2 k_B T} \right) \Gamma\left(\frac{3}{4} + i \frac{\alpha}{2\pi} - i \frac{\hbar \epsilon}{\pi 2 k_B T} \right)}{\Gamma\left(\frac{3}{2} \right)}, \tag{A18}$$

where the dimensionless constants are

$$B_c = \frac{\Lambda}{\sqrt{1 + e^{-2\alpha}}}, \quad B_\psi = \frac{\sqrt{p} \pi J^2}{2 V^2 \Lambda \sqrt{1 + e^{-2\alpha}}}, \tag{A19}$$

$$\Lambda = \left(\frac{(1 - 2p)}{\cos 2\theta} \right)^{\frac{1}{4}}, \quad \alpha = \ln \left[\tan \left(\frac{\pi}{4} + \theta \right) \right]. \tag{A20}$$

These are obtained from the general solution in Ref. [11] by rescaling p and V in the saddle-point equations [Eq. (B14)]. Upon substituting the low-energy forms of the spectral densities in Eq. (A16), the explicit dependence on temperature cancels and the expression reduces to a dimensionless integral over four gamma functions. As discussed in Ref. [41], where a similar calculation was considered, this integral can be evaluated as

$$\int_{-i\infty}^{i\infty} ds \, \Gamma(\alpha + s) \Gamma(\beta + s) \Gamma(\gamma - s) \Gamma(\delta - s) = 2\pi i \frac{\Gamma(\alpha + \gamma) \Gamma(\alpha + \delta) \Gamma(\beta + \gamma) \Gamma(\beta + \delta)}{\Gamma(\alpha + \beta + \gamma + \delta)}, \tag{A21}$$

where $\mathrm{Re}(\alpha, \beta, \gamma, \delta) > 0$ according to Eq. 6.412 of Ref. [42]. After some straightforward algebra, the dc conductance reduces to

$$G(\omega \to 0, T, \mu) = \left(\frac{e^2}{2h} \sqrt{NM} \right) \left[\pi \sin \left(\frac{\pi}{2} + 2\theta \right) \right] \sqrt{p}, \tag{A22}$$

valid for $p < p_c = \frac{1}{2}$. As initially discussed in the context of overscreened Kondo impurities [25] and subsequently in SYK models [3,11], the phase θ is related to p and the total filling on dot and lead (end points) via a form of Luttinger's theorem. At particle-hole symmetry, $\theta = 0$ for all p.

We follow a similar procedure to determine the zero-temperature tunneling conductance from

$$\lim_{T\to 0} G = \frac{e^2V^2\sqrt{NM}\pi^2}{h\omega}\int_{-|\omega|}^{0} d\epsilon[\rho_c(\epsilon)\rho_\psi(\epsilon+\omega) + \rho_\psi(\epsilon)\rho_c(\epsilon+\omega)], \quad \omega \geqslant 0. \tag{A23}$$

The spectral densities in the conformal regime $\hbar\omega \ll k_B T^*$ on the NFL side can be obtained by using Sterling's formula [43] for the gamma functions in Eqs. (A17) and (A18) or by using an analytical continuation from the ansatz in Ref. [3]:

$$\rho_c(\epsilon, T=0) = \frac{1}{\pi}\frac{\Lambda}{\sqrt{J\hbar|\epsilon|}}L(\epsilon), \tag{A24}$$

$$\rho_\psi(\epsilon, T=0) = \frac{1}{\pi}\frac{\sqrt{p}\sqrt{J\hbar|\epsilon|}}{V^2\Lambda}L(\epsilon), \tag{A25}$$

where

$$L(\epsilon) = \begin{cases} \sin(\pi/4+\theta), & \epsilon \geqslant 0 \\ \cos(\pi/4+\theta), & \epsilon < 0. \end{cases} \tag{A26}$$

Substitution into the zero-temperature expression for the conductance and use of Eq. 3.192 in Ref. [42] gives

$$G(\omega, T\to 0, \mu) = \left(\frac{e^2}{2h}\sqrt{NM}\right)\left[\pi \sin\left(\frac{\pi}{2}+2\theta\right)\right]\sqrt{p}, \tag{A27}$$

valid for $p < p_c = \frac{1}{2}$. This is identical to the dc conductance in Eq. (A22). The dimensionless conductance $g_0(p)$ discussed in the main text follows from these expressions. Note that these results correspond to the *leading* contribution in the emergent conformal-invariant regime on the NFL side. We ignored corrections $\sim(T/T^*)$, $(\hbar\omega/k_B T^*)$ due to leading irrelevant terms which break this symmetry [3].

In the FL regime at particle-hole symmetry, we determine the leading contribution to the conductance by substituting Eqs. (B15) and (B16) into Eq. (A23):

$$G(\omega, T\to 0, \mu = 0, p > 1/2) = \left(\frac{e^2}{2h}\sqrt{NM}\right)\frac{2}{\sqrt{p}}. \tag{A28}$$

The same expression holds in the $\omega \to 0$ limit as obtained by substituting the forms in Eqs. (B15) and (B16) into (A16).

3. Corrections to the universal conductance

In the main text, we discussed corrections to the conformal-invariant NFL and FL solutions which are linear and quadratic in temperature, respectively. Here, we support these statements with numerical results.

In Fig. 14(a), we plot deviations from the universal conductance $g_0(p < \frac{1}{2})$ [Eq. (15)] in the NFL regime, for $p = 0.1$, versus temperature. The linear dependence is apparent. Corrections to the universal conductance $g_0(p > \frac{1}{2})$ in the FL regime, for $p = 0.8$, versus temperature are shown in Fig. 14(b). We see that they scale quadratically with temperature.

APPENDIX B: LARGE-(N, M) SADDLE-POINT SOLUTIONS

1. Saddle-point equations

Following Ref. [17], we write the path integral for our model, ignoring the extended leads [Eq. (3)] and obtain an effective action after disorder averaging:

$$\overline{Z} = \int \mathcal{D}[\psi_{L/R}, \overline{\psi}_{L/R}, c, \overline{c}]e^{iS}, \tag{B1}$$

where the Grassmann fields correspond to left and right lead end points and dot, respectively. The real-time action is defined on the Keldysh contour [44] and can be written as a sum of contributions from the left/right leads, dot, and coupling between them:

$$S = S_L + S_R + S_D + S_{LD} + S_{RD}, \tag{B2}$$

$$S_{L/R} = \sum_s\sum_\alpha\int dt\{\overline{\psi}_{\alpha s}(t)s[i\partial_t+\mu]\psi_{\alpha s}(t)\} - \sum_{ss'}\int\int dt\,dt'\left\{ss'\frac{it^2}{2M}\left(\sum_\alpha\overline{\psi}_{\alpha s}(t)\psi_{\alpha s'}(t')\right)\left(\sum_\beta\overline{\psi}_{\beta s'}(t')\psi_{\beta s}(t)\right)\right\}, \tag{B3}$$

$$S_D = \sum_s\sum_i\int dt\{\overline{c}_{is}(t)s[i\partial_t+\mu]c_{is}(t)\} + \sum_{ss'}\int\int dt\,dt'\left\{ss'\frac{iJ^2}{4N^3}\left(\sum_i\overline{c}_{is}(t)c_{is'}(t')\right)^2\left(\sum_j\overline{c}_{js'}(t')c_{js}(t)\right)^2\right\}, \tag{B4}$$

$$S_{L/RD} = -\sum_{ss'}\int\int dt\,dt'\left\{ss'\frac{iV^2}{\sqrt{NM}}\left(\sum_i\overline{c}_{is}(t)c_{is'}(t')\right)\left(\sum_\alpha\overline{\psi}_{\alpha s'}(t')\psi_{\alpha s}(t)\right)\right\}. \tag{B5}$$

We suppressed the L/R indices on the lead fields for clarity. The integrals run from $-\infty$ to ∞ and the index $s = \pm 1$ labels the forward and backward directions on the Keldysh contour [17]. We introduce the fields $G_{c,\psi}$ together with the Lagrange

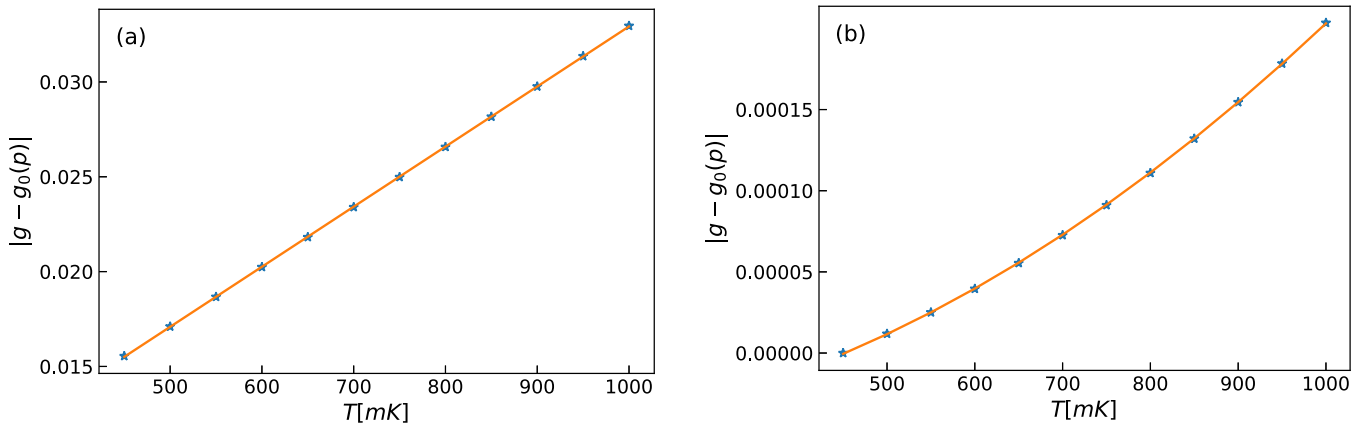

FIG. 14. (a) Corrections to the universal dc conductance $g_0(p)$ in the NFL regime [Eq. (15) in the main text, for $\omega \to 0$], for $p = 0.1$, versus temperature. The linear dependence is apparent. (b) Same as (a) in the FL regime, for $p = 0.8$, versus temperature. A quadratic dependence is obtained.

multipliers $\Sigma_{c,\psi}$:

$$\int \mathcal{D}[G_c, \Sigma_c] \exp\left(N \sum_{ss'} \int\int dt\, dt' \left\{\Sigma_{c,ss'}(t,t')\left[G_{c,s's}(t',t) - \frac{i}{N}\sum_i \bar{c}_{is}(t) c_{is'}(t')\right]\right\}\right) = 1,$$

$$\int \mathcal{D}[G_\psi, \Sigma_\psi] \exp\left(M \sum_{ss'} \int\int dt\, dt' \left\{\Sigma_{\psi,ss'}(t,t')\left[G_{\psi,s's}(t',t) - \frac{i}{M}\sum_i \bar{\psi}_{is}(t) \psi_{is'}(t')\right]\right\}\right) = 1.$$

The resulting action is

$$S_{L/R} = \sum_{ss'}\sum_{\alpha} \int\int dt\, dt' \left\{\bar{\psi}_{\alpha s}(t)\left[\sigma^z_{ss'}\delta_{tt'}(i\partial_t + \mu) - \Sigma_{\psi,ss'}(t,t')\right]\psi_{\alpha s'}(t')\right\}$$
$$+ \sum_{ss'} \int\int dt\, dt' \left\{iss' \frac{Mt^2}{2} G_{\psi,s's}(t',t) G_{\psi,ss'}(t,t') - iM\Sigma_{\psi,ss'}(t,t') G_{\psi,s's}(t',t)\right\}, \tag{B6}$$

$$S_D = \sum_{ss'}\sum_{i} \int\int dt\, dt' \left\{\bar{c}_{is}(t)\left[\sigma^z_{ss'}\delta_{tt'}(i\partial_t + \mu) - \Sigma_{c,ss'}(t,t')\right]c_{is'}(t')\right\}$$
$$+ \sum_{ss'} \int\int dt\, dt' \left\{iss' \frac{NJ^2}{4} G^2_{c,s's}(t',t) G^2_{c,ss'}(t,t') - iN\Sigma_{c,ss'}(t,t') G_{c,s's}(t',t)\right\}, \tag{B7}$$

$$S_{L/RD} = \sum_{ss'} \int\int dt\, dt' \{iss'\sqrt{NM}V^2 G_{c,s's}(t',t) G_{\psi,ss'}(t,t')\}. \tag{B8}$$

After integrating out the fermions, we find the saddle point of the action

$$\frac{\delta S}{\delta G_{a,ss'}(t,t')} = 0, \quad \frac{\delta S}{\delta \Sigma_{a,ss'}(t,t')} = 0, \tag{B9}$$

where a stands for c and ψ indices for dot and leads, respectively. We drop the dependence on two time indices and obtain the saddle-point equations that follow from Eq. (B9):

$$\Sigma_{c,ss'}(t) = ss' J^2 G^2_{c,ss'}(t) G_{c,s's}(-t) + ss'\sqrt{p}V^2 G_{\psi,L,ss'}(t) + ss'\sqrt{p}V^2 G_{\psi,R,ss'}(t), \tag{B10}$$

$$\Sigma_{\psi,L/R,ss'}(t) = ss' t^2 G_{\psi,L/R,ss'}(t) + ss' \frac{V^2}{\sqrt{p}} G_{c,ss'}(t), \tag{B11}$$

where $p = M/N$. These are supplemented by the (matrix) Dyson equation for the frequency-dependent Green's functions which we obtain from (B9):

$$G_{a,ss'}(\omega) = [\sigma^z(\omega + \mu) - \Sigma]^{-1}_{a,ss'}. \tag{B12}$$

The matrix equations are cast in a Keldysh basis for retarded, advanced, and Keldysh components via the standard transformation [44]. In equilibrium, a "fluctuation-dissipation" relation [45] is imposed:

$$G^K(\omega) = 2i \tanh\left(\frac{\beta\omega}{2}\right)\mathrm{Im}G^R(\omega). \tag{B13}$$

Recall that we consider identical left and right leads. In this case, $G_{\psi,L} = G_{\psi,R}$ the saddle-point equations [Eqs. (B10) and (B11)] are formally identical to those in Ref. [11] after a simple rescaling of V and p:

$$V^2 \to \sqrt{2}V^2, \quad p \to 2p. \tag{B14}$$

Consequently, the phase transition occurs at $p_c = 1/2$.

2. Numerical solution

The saddle-point Eqs. (B10)–(B12) are solved by direct numerical iteration with Green's functions defined on a discrete set of 2^{16} time points, with an ultraviolet cutoff of $10J$ in the frequency domain. Since the saddle-point equations have a simpler form in time while the frequency representation is more natural for Dyson's equation, we used NFFT [46] library for Python to switch between the time and frequency representations of the Green's functions at each iteration. Using the NFFT with nonequispaced frequencies allows for an effective sampling the of the spectral weights near zero and shorter computation times. The plots shown in the main text are determined for fixed $V = t = \frac{J}{2}$ unless stated otherwise.

3. Spectral densities in equilibrium

In equilibrium, the spectral densities in the conformal-invariant NFL regime were shown in Eqs. (A17) and (A18). Our numerical solutions are consistent with these forms. In Fig. 15(a) we plot the spectral densities for the dot electrons ρ_c scaled by $\sqrt{Jk_BT}$, for $p = 0.1 < p_c$, at particle-hole symmetry, for several temperatures, versus the dimensionless parameter $\hbar\omega/k_BT$. We see scaling collapse for values of the abscissa below roughly 10^2. Above this cutoff, clear departures from scaling associated with the crossover scale k_BT^* are apparent. Immediately below it, the curves follow a $1/\sqrt{x}$ dependence corresponding to the high-frequency limit of Eq. (A17) in the conformal regime, as can be checked by using Sterling's formula (Eq. 6.3.17 in Ref. [43]). For $\hbar\omega/k_BT \ll 1$, the divergence in the high-frequency regime is cut off by a peak of width $\sim T$. A similar scaling holds for the lead end-point spectral densities ρ_ψ as shown in Fig. 15(b). In either case, we also observe slight departures from the ideal scaling of the conformal-invariant solutions due to corrections $\sim T/T^*$.

At particle-hole symmetry, the leading spectral densities in the FL regime can be obtained from Ref. [11] via the transformation defined in Eq. (B14):

$$\rho_c = \frac{1}{\pi}\frac{1}{\sqrt{2p-1}}\frac{t}{\sqrt{2}V^2}, \tag{B15}$$

$$\rho_\psi = \frac{1}{\pi}\sqrt{\frac{2p-1}{2p}}\frac{1}{t}. \tag{B16}$$

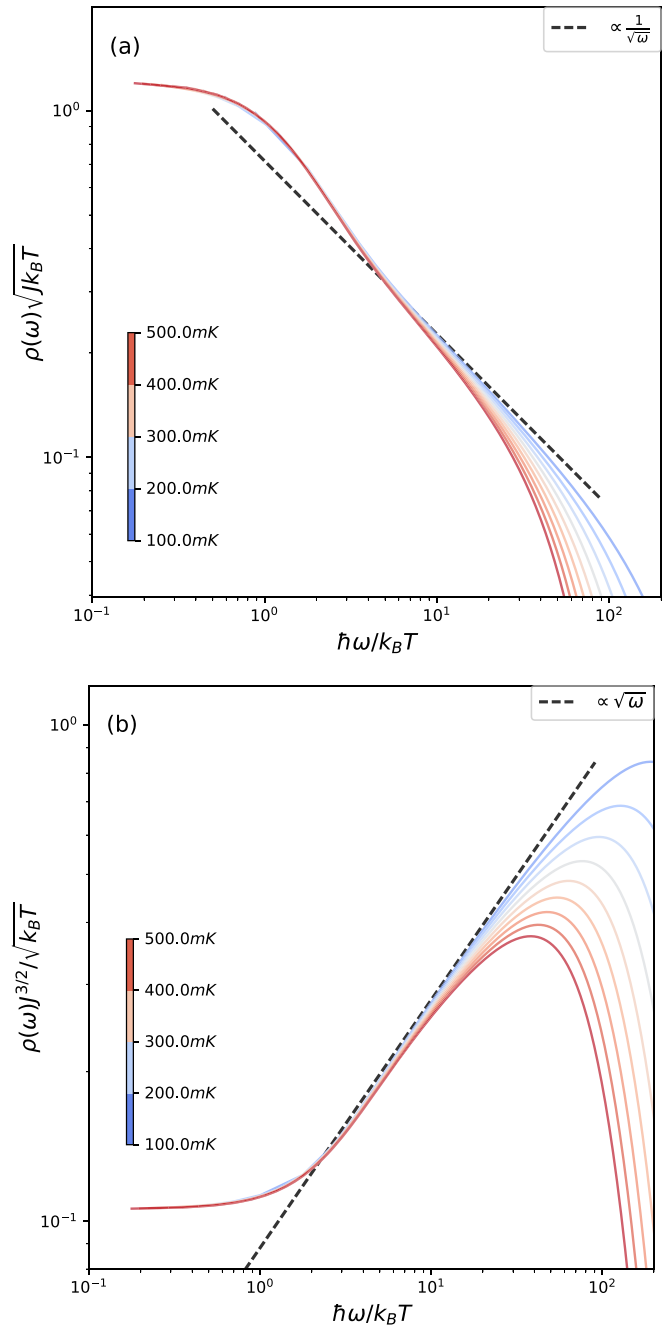

FIG. 15. (a) Spectral density ρ_c for the dot electrons scaled by $\sqrt{k_BT}$, for several temperatures, at $p = 0.1 < p_c$ and particle-hole symmetry, as a function of the dimensionless parameter $\hbar\omega/k_BT$. The curves show scaling collapse below values of the abscissa of $O(10^2)$. This regime corresponds to the leading behavior for conformal-invariant solutions in Eq. (A17), as indicated by the dashed line. For lower temperatures, the divergence is cut off by a finite peak of width $\sim T$. (b) Same as (a) for the lead end-point spectral functions in Eq. (A18).

APPENDIX C: TUNNELING CURRENT FOR STATIC BIAS BEYOND LINEAR RESPONSE

We determine the steady-state current by allowing the biases defined in Eq. (A2) to be arbitrarily large. The disorder-averaged currents *out* of the left and right leads, respectively,

are obtained from Eq. (A7). Recall that we consider couplings to the L/R leads which are statistically identical with equal variance V^2. We determine the current for arbitrary applied bias U and to all orders in the coupling constants t, V, J by keeping contributions to leading order in N, M. The diagrammatic expansion is evaluated using a contour-ordered formalism, followed by an analytic continuation to real times. For an in-depth discussion of this we refer the reader to Refs. [32,47]. More specifically, we allow for noninteracting, disorder-free leads at $t \to -\infty$ which are in equilibrium with large reservoirs at shifted chemical potentials $\mu \pm eU/2$ for left and right leads, respectively. We subsequently turn on all couplings adiabatically. In practice, we ignore the initial state of the dot. This is a commonly employed approximation when calculating steady-state currents [32,48]. In addition, we assume that for sufficiently long times, the leads reach equilibrium with the large reservoirs. Likewise, we ignore the time dependence of the current.

To calculate the steady-state current we require the $<$ Green's functions

$$G_I^<(t,t') = i\,\langle \psi_{L\alpha}^\dagger(t) c_i(t')\rangle, \tag{C1}$$

$$G_{II}^<(t,t') = i\,\langle c_i^\dagger(t)\psi_{L\alpha}(t')\rangle. \tag{C2}$$

Consider the related, contour-ordered Green's functions

$$G_{C,I}(\tau,\tau') = -\,i\,\overline{\frac{V_{Li\alpha}^*}{(NM)^{1/4}}\,\langle T_C c_\tau(t)\psi_{L\alpha}^\dagger(\tau')\rangle}, \tag{C3}$$

$$G_{C,II}(\tau,\tau') = -\,i\,\overline{\frac{V_{Li\alpha}}{(NM)^{1/4}}\,\langle T_C \psi_{L\alpha}(\tau) c_i^\dagger(\tau')\rangle}, \tag{C4}$$

defined on the contour extending from $-\infty$ and back, passing through τ and τ' once [32]. T_C stands for ordering along the contour. These functions coincide with the real-time $<$ propagators when τ and τ' are on the upper and lower branch of the Keldysh contour [44], respectively. As discussed in a number of references [32,44,47], the contour-ordered Green's functions allow for a straightforward application of Wick's theorem. We note that this procedure entails no difficulties with respect to disorder averaging. One can check that the diagrammatic expansion in Fig. 16, followed by analytical continuation [32] to the real axis, reproduces the saddle-point equations in equilibrium [Eqs. (B10) and (B11)], within minus signs for $\Sigma_{c,\psi}^{\langle,\rangle}$. The difference between the two approaches is due to a convention in defining the self-energies which appear in the saddle-point derivation [17], and is otherwise innocuous. In order to keep the sign convention common in the literature on transport through quantum dots [29,32,44], in this section we use the more typical convention for the signs of the $\langle,\rangle$ self-energies.

Once the functions $G_{I,II}^C(\tau,\tau')$ are known, we proceed to determine their real-time counterparts via the same analytical continuation.

Using the diagrammatic expansion in Fig. 16, we determine

$$G_{C,I}(\tau,\tau') = \frac{V^2}{\sqrt{NM}}\delta_{\alpha\beta}\delta_{ij}\int_C d\tau_1 G_{C,c,ij}(\tau,\tau_1) \times G_{C,\psi L/R,\alpha\beta}(\tau_1,\tau'), \tag{C5}$$

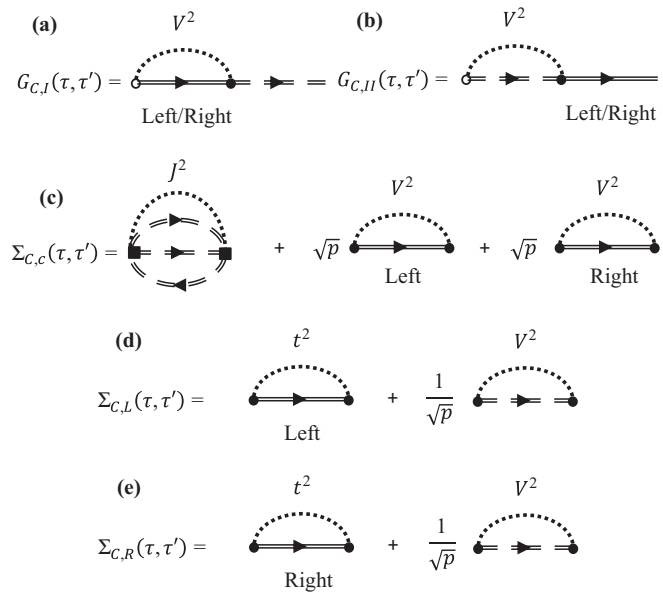

FIG. 16. Contour-ordered diagrammatic expansions for the disorder-averaged tunneling current to leading order in N, M and to all orders in t, V, J. The dashed, double line represents the fully dressed dot propagator, while the continuous, double lines stand for the fully dressed left/right lead propagators. Internal vertices are indicated by filled symbols, while the external vertex for the current is denoted an empty circle. Dotted lines connecting vertices represent disorder averages. (a) The contour-ordered Green's function $G_{C,I}$ in Eq. (C4) for either left or right lead. (b) Same as (a) for $G_{C,II}$ in Eq. (C3). (c) Diagrams which determine the self-energy for the dot to leading order in N, M. (d), (e) Same as (c) for the left and right leads. Note that the saddle-point equations in Eqs. (B10) and (B11) can also be obtained via analytical continuation [32]. The effect of the bias is included via the unperturbed lead propagators.

$$G_{C,II}(\tau,\tau') = \frac{V^2}{\sqrt{NM}}\delta_{\alpha\beta}\delta_{ij}\int_C d\tau_1 G_{C,\psi L/R,\alpha\beta}(\tau,\tau_1) \times G_{C,c,ij}(\tau_1,\tau'), \tag{C6}$$

where factors of $1/\sqrt{NM}$ are due to the definition of the hybridization V [Eq. (3)]. We analytically continue these expressions onto the real axis according to the following rule [32,47]:

$$C = \int_C d\tau_1 AB \to C^< = \int_t dt_1 [A^R B^< + A^< B^A], \tag{C7}$$

where the R, A indices stand for the retarded and advanced components. The corresponding expression for the current from the left or right leads into the dot is

$$\langle I_{L/R}\rangle = \frac{e}{\hbar}V^2\sqrt{NM}\int_{-\infty}^{\infty} dt_1\big[G_c^R(t,t_1)G_{\psi L/R}^<(t_1,t^+) + G_c^<(t,t_1)G_{\psi L/R}^A(t_1,t^+) - G_{\psi L/R}^R(t,t_1)G_c^<(t_1,t^+) - G_{\psi L/R}^<(t,t_1)G_c^A(t_1,t^+)\big]. \tag{C8}$$

Note that this expression can also be obtained by using diagram rules directly in the matrix formulation [44]. The factor of $\sqrt{NM}$ is due to the summation over the α, i indices

[Eq. (A7)]. As we are considering the steady-state current $t \gg t_0 = -\infty$, for a static bias, and since the interactions are turned on adiabatically, we can consider only the difference between the time arguments. We obtain the steady-state current

$$\langle I_{L/R}\rangle = \frac{e}{\hbar}V^2\sqrt{NM}\int\frac{d\omega}{2\pi}\big\{G^<_{\psi L/R}(\omega)\big[G^R_c(\omega)-G^A_c(\omega)\big] - G^<_c(\omega)\big[G^R_{\psi L/R}(\omega)-G^A_{\psi L/R}(\omega)\big]\big\}. \tag{C9}$$

This is the central result of this section.

Note that our expression for the tunneling current (C9) is analogous to cases involving an interacting dot coupled to *noninteracting leads* [28,32,49]. The important difference is due to the disordered coupling between leads and dot $V_{i,\alpha}$ which implies that both dot and lead Green's functions must be determined self-consistently. Indeed, the single-particle propagators which enter our expression for the current are determined via the same set of saddle-point equations encountered in equilibrium [Eqs. (B10) and (B11), see Fig. 16], with the additional contribution due to the biases.

Before proceeding to a discussion of the numerical implementation, we note a number of important points. First, the current vanishes in equilibrium, as expected. This can be seen by using the equilibrium forms for the $<$ Green's functions (Eq. 2.160 of Ref. [29]), which are given by

$$G^< = 2\pi i f(\omega)\rho(\omega). \tag{C10}$$

The components which enter this expression are the Fermi-Dirac function $f(\omega)$ and the spectral density $\rho(\omega)$. When the bias is set to zero, the left and right leads have the same chemical potential. Substitution of the equilibrium forms into the expression for the current ensures that the latter vanishes, as expected.

Second, we consider the condition for charge conservation on the dot in the steady-state regime:

$$I_L + I_R = 0. \tag{C11}$$

Using the well-known analytical property [29,44] $G^> - G^< = G^R - G^A$, the conservation of charge is equivalent to

$$\int d\omega\{G^>_c(\omega)[V^2G^<_{\psi L}(\omega)+V^2G^<_{\psi R}(\omega)] - G^<_c(\omega)[V^2G^>_{\psi L}(\omega)+V^2G^>_{\psi R}(\omega)]\} = 0. \tag{C12}$$

From the diagrams shown in Fig. 16 we obtain for the dot self-energy

$$\Sigma^{\langle,\rangle}_c = \sqrt{p}V^2[G^{\langle,\rangle}_L + G^{\langle,\rangle}_R] + \Sigma^{\langle,\rangle}_{\rm int}, \tag{C13}$$

where $\Sigma_{\rm int} \sim J^2$ is the proper self-energy of the dot due to interactions. Following Eq. 12.28 in Ref. [32], we solve for $V^2[G^{\langle,\rangle}_L + G^{\langle,\rangle}_R]$ in terms of the self-energies, substitute into the charge-conservation condition, and obtain

$$\int d\omega\{G^>_c[\Sigma^<_c - \Sigma^<_{\rm int}] - G^<_c[\Sigma^>_c - \Sigma^>_{\rm int}]\} = 0. \tag{C14}$$

In our case, the Keldysh equation for $G^<_c$ reads as [32]

$$G^<_c = G^R\Sigma^<_c G^A_c. \tag{C15}$$

This differs from the full expression (Eq. 2.159 in Ref. [29]) by terms proportional to $G^{<,(0)}_c$. These functions represent the initial correlations at $t \to -\infty$ which are ignored in our calculations (see, for example, comment 33 in Ref. [48]). This is a standard approximation in the context of transport through interacting quantum dots [32]. The simplified Keldysh equation implies that

$$G^>_c\Sigma^<_c - G^<_c\Sigma^>_c = 0. \tag{C16}$$

Therefore, conservation of charge reduces to the condition involving the self-energy of the dot due to interactions

$$\int d\omega\{G^<_c\Sigma^>_{\rm int} - G^>_c\Sigma^<_{\rm int}\} = 0, \tag{C17}$$

which is also well known in the context of transport through interacting Anderson impurity models [49]. We show that our saddle-point approximation, as given by the self-consistent diagrams in Fig. 16, ensures that this condition is satisfied *for each frequency*. At saddle point, the self-energy due to interactions is

$$\Sigma^{\langle,\rangle}_J(t) = J^2[G^{\langle,\rangle}_c(t)]^2G^{>,<}_c(-t). \tag{C18}$$

Fourier transforming and substituting into the condition for charge conservation [Eq. (C17)] we obtain

$$\int d\omega\int d\omega_{1,2,3}\delta(\omega_1+\omega_2-\omega_3-\omega) \times [G^<_c(\omega)G^>_c(\omega_1)G^>_c(\omega_2)G^<_c(\omega_3) - G^>_c(\omega)G^<_c(\omega_1)G^<_c(\omega_2)G^>_c(\omega_3)] = 0. \tag{C19}$$

We can relabel the indices in the second term as $(\omega_1,\omega_2) \leftrightarrow (\omega,\omega_3)$. The even δ function of the same term is invariant under the transformation. Thus, our approximation satisfies the conserving condition for each frequency ω.

This important point allows us to determine an effective distribution function $F(\omega)$ for the dot out of equilibrium. To do so, we rewrite the charge conservation as a sum of left and right currents [Eq. (C9)]

$$\langle I_L + I_R\rangle = \frac{e}{\hbar}V_L^2\sqrt{NM}\int\frac{d\omega}{2\pi}\big\{\big[G^R_c(\omega)-G^A_c(\omega)\big] \times [G^<_{\psi L}(\omega)+G^<_{\psi R}(\omega)] - G^<_c(\omega)\big[G^R_{\psi L}(\omega)-G^A_{\psi L}(\omega)+G^R_{\psi R}(\omega) - G^A_{\psi R}(\omega)\big]\big\}. \tag{C20}$$

Since the integrand vanishes for all frequencies, we can readily solve for

$$G^<_c(\omega) = \frac{G^<_{\psi L}(\omega)+G^<_{\psi R}(\omega)}{G^R_{\psi L}(\omega)-G^A_{\psi L}(\omega)+G^R_{\psi R}(\omega)-G^A_{\psi R}(\omega)} \times \big[G^R_c(\omega)-G^A_c(\omega)\big]. \tag{C21}$$

We assume that the leads are maintained in thermal equilibrium at shifted chemical potentials throughout the temporal evolution, implying the equilibrium forms [Eq. (C10)] for either left/right leads with Fermi-Dirac distributions

$$f_{L/R}(\omega) = \frac{1}{e^{\beta(\hbar\omega-\mu\pm eU/2)}+1}, \tag{C22}$$

where U is the applied bias. We obtain the distribution function for the dot out of equilibrium according to

$$G_c^<(\omega) = 2\pi i F_c(\omega)\rho_c(\omega), \tag{C23}$$

$$F_c(\omega) = \frac{f_L(\omega)\rho_L(\omega) + f_R(\omega)\rho_R(\omega)}{\rho_L(\omega) + \rho_R(\omega)}. \tag{C24}$$

To summarize, we employ the following procedure:

(1) The lead end points are kept in thermal equilibrium with large reservoirs at shifted chemical potentials according to the distribution in Eq. (C22). Likewise, we include the bias terms $\sim \pm eU/2$ in the Hamiltonian for left and right leads, respectively, in accordance with the standard procedure for systems under an applied constant field (Eq. 10-7 in Ref. [50]).

(2) The saddle-point equations [Eqs. (B10) and (B11)] in the presence of the biases are solved numerically by imposing the form in Eqs. (C23) and (C24). This step determines the local spectral densities for the lead end points $\rho_{L,R}$, and the spectral density for the dot ρ_c together with the distribution function F_c.

(3) The tunneling current is determined according to Eq. (C9) via the functions $G^<_{L/R/c}$ and the spectral functions.

APPENDIX D: WEAK-TUNNELING APPROXIMATION

In order to determine the disorder-averaged current in the weak-tunneling approximation, we employ the standard tunneling conductance formula [29]. The latter gives the current as a convolution of the spectral densities of the lead and the dot calculated with their mutual coupling set to zero. After Gaussian averaging over the couplings V_{ij}, we obtain the following formula for our setup:

$$\langle I_{\rm WT}\rangle = 4\pi^2 \frac{e}{h} V^2 \sqrt{NM} \int_{-\infty}^{\infty} \rho_\psi\left(\epsilon + \frac{eU}{\hbar}\right)\rho_c(\epsilon) \times \left[f(\epsilon) - f\left(\epsilon + \frac{eU}{\hbar}\right)\right] d\epsilon. \tag{D1}$$

We assumed that both leads and dot are kept in thermal equilibrium at the same temperature with separate, large reservoirs. However, we assume that the chemical potentials for the leads and dot are shifted due to a finite bias. Furthermore, we assume that the current from left lead to dot is equal to the current from dot to right lead, as in the previous sections.

The spectral functions are obtained from the retarded Green's function of the SYK_4 model [3]. At particle-hole symmetry and nonzero temperature, the dot Green's function is given by

$$G^R = \frac{-iC}{\sqrt{2\pi T}} \frac{\Gamma(1/4 - i\beta\hbar\omega/2\pi)}{\Gamma(3/4 - i\beta\hbar\omega/2\pi)},$$

which gives the spectral density $\rho_c = -\frac{1}{\pi}{\rm Im}G^R$,

$$\rho_c \propto \frac{1}{\sqrt{T}} |\Gamma(1/4 + i\beta\hbar\omega/2\pi)|^2 \cosh\left(\frac{\beta\hbar\omega}{2}\right).$$

The Green's function for the lead can be obtained by setting $V = 0$ in saddle-point equations given in Appendix B1 and solving for the lead Green's function. One obtains

$$\rho_\psi = \frac{1}{\pi t}{\rm Re}\sqrt{1 - \left(\frac{\hbar\omega}{2t}\right)^2}.$$

Substituting these expressions into Eq. (D1) we find

$$\langle I_{\rm WT}\rangle \simeq e\frac{V^2}{t}\sqrt{NM}\frac{1}{\sqrt{T}} \times \int_{-\infty}^{\infty} |\Gamma(1/4 + i\beta\hbar\epsilon/2\pi)|^2 \cosh\left(\frac{\beta\hbar\epsilon}{2}\right) \times \left[f(\epsilon) - f\left(\epsilon + \frac{eU}{\hbar}\right)\right] d\epsilon,$$

where we assumed that the lead spectral density $\rho_\psi \approx \frac{1}{\pi t}$ is flat. This will be valid when the range of integration $|\epsilon| \ll t$ which we expect to be true at reasonable bias voltages. We estimate this integral in two limits:

(a) $eU \ll k_B T$. In this case Fermi factors reduce effectively to a derivative and we have

$$\lim_{eU\to 0} \frac{f(\epsilon) - f\left(\epsilon + \frac{eU}{\hbar}\right)}{\frac{eU}{\hbar}} = \frac{\hbar\beta}{4\cosh^2(\beta\hbar\epsilon/2)}.$$

The integral above becomes

$$\langle I_{\rm WT}\rangle \simeq e\frac{V^2}{t}\sqrt{NM}\frac{1}{\sqrt{T}} \times eU \int_{-\infty}^{\infty} \frac{|\Gamma(1/4 + i\beta\hbar\epsilon/2\pi)|^2}{4\cosh(\beta\hbar\epsilon/2)} d(\beta\hbar\epsilon).$$

Substitution $y = \beta\hbar\epsilon$ reduces the integral to a dimensionless constant. From this expression we can easily extract the dependence on the bias voltage and temperature

$$\langle I_{\rm WT}\rangle \propto \frac{eU}{\sqrt{T}} \quad (eU \ll k_B T). \tag{D2}$$

(b) $eU \gg k_B T$. In this case, Fermi factors introduce limits to the integral, as they are effectively step functions. We have

$$\langle I_{\rm WT}\rangle \simeq e\frac{V^2}{t}\sqrt{NM}\frac{1}{\sqrt{T}} \times \frac{1}{\beta}\int_{-\beta eU}^{0} |\Gamma(1/4 + i\beta\epsilon/2\pi)|^2 \cosh\left(\frac{\beta\epsilon}{2}\right) d(\beta\epsilon).$$

For $\beta\epsilon \gg 1$ the integrand can be approximated as

$$|\Gamma(1/4 + i\beta\epsilon/2\pi)|^2 \cosh\left(\frac{\beta\epsilon}{2}\right) \simeq \frac{1}{\sqrt{|\beta\epsilon|}}.$$

The integral can be estimated as

$$\langle I_{\rm WT}\rangle \propto e\frac{V^2}{t}\sqrt{NM}\frac{1}{\sqrt{\beta T}}\sqrt{eU},$$

from which we can extract the dependence of the average tunneling current on the external parameters

$$\langle I_{\rm WT}\rangle \propto \sqrt{eU} \quad (eU \gg k_B T). \tag{D3}$$

It is important to recall that we assumed $\epsilon \ll t$ above, which implies that the results will be valid only when the temperature and the bias are much smaller than t.

To summarize, we found that the weak-tunneling current $I_{\rm WT}$ is given by

$$\langle I_{\rm WT}\rangle \propto \begin{cases} eU/\sqrt{T} & (eU \ll k_B T), \\ \sqrt{eU} & (eU \gg k_B T). \end{cases} \tag{D4}$$

APPENDIX E: SADDLE-POINT EQUATIONS IN THE PRESENCE OF EXPLICIT COUPLING TO EXTENDED LEADS

The discussion in the main text involved an *effective local model* [Eq. (3)] for the junction between lead end points and graphene dot. We assumed that the lead *end points* are dominated by local disorder scattering. Consequently, they were described by a local SYK_2 Hamiltonian. As such, we effectively ignored a coupling to the bulk of the leads. This approximation is expected to be valid provided that the phase diagram in Fig. 2 is essentially unchanged when a coupling to the bulk of the leads is included in the effective model for the junction. We find that this is indeed the case for quasi-one-dimensional ballistic leads.

We model the extended leads as a set of M-independent, semi-infinite noninteracting chains, labeled by an index α. Each of the chains includes simple nearest-neighbor hopping and is coupled to *a single end-point state* $\psi_{L/R,\alpha}$, as indicated by Hamiltonian (6). In the absence of interactions, the coupling to the leads can be included in the effective local model for the junction to all orders by a redefinition of the bare lead end-point propagator

$$G^0_{\psi,L/R}(i\omega_n) \to \tilde{G}^0_{\psi,L/R}(i\omega_n) = \frac{1}{i\omega_n + \mu - \Sigma_{EL/R}(i\omega_n)}, \tag{E1}$$

while the saddle-point equations [Eqs. (B10) and (B11)] preserve their form. This can be seen via expanding the diagrams in Figs. 16(b) and 16(c) and inserting all corrections due to $H_{EL/R}$ in all of the bare lead propagators (full lines).

The self-energies due to the additional coupling to the extended leads are given by

$$\Sigma_{EL/R,\alpha}(i\omega_n) = (t_{-1/1,\alpha})^2 \int d\epsilon \frac{\rho_{loc,L/R,\alpha}(\epsilon)}{i\omega_n - \epsilon}. \tag{E2}$$

These depend on the local density of states at sites $-1, 1$, $\rho_{{\rm loc},L/R,\alpha}(\epsilon) = -(1/\pi){\rm Im}G^R_{i=-\mp 1}(\epsilon)$.

Our goal is to account for the effect of the bulk of the leads in an effective model for the junction. In a manner analogous to treatments of Anderson impurity models coupled to a bath of conduction electrons [31], we approximate $\rho_{\rm loc}$ by a constant density of states near the end of a semi-infinite chain [51]. Furthermore, we assume that the chains are identical and ignore the α index. The local density of states is then given by

$$\rho_{{\rm loc},L/R,\alpha}(\epsilon) = \rho_E, \quad |\epsilon| \ll D \tag{E3}$$

where $D \gg V, J$ is a cutoff of the order of the bandwidth of the extended leads.

For simplicity, we relabel $t_{-1/1} = t_E$. By substituting ρ_E in Eq. (E2), and continuing to real frequencies we obtain the retarded self-energy due to coupling to the extended leads

$${\rm Re}\Sigma^R_E(\omega) = \rho_E t_E^2 \ln\left|\frac{\omega + D}{\omega - D}\right|, \tag{E4}$$

$${\rm Im}\Sigma^R_E(\omega) = -\pi\rho_E t_E^2. \tag{E5}$$

In equilibrium, the Keldysh component is given by [44]

$$\Sigma^K_E(\omega) = 2i \tanh\left(\frac{\beta\omega}{2}\right){\rm Im}\Sigma^R_E(\omega). \tag{E6}$$

These components are added to the self-energies in the matrix Dyson equation [Eq. (B12)] and solved together with the saddle-point equations numerically.

[1] S. Sachdev and J. Ye, Phys. Rev. Lett. **70**, 3339 (1993).
[2] A. Kitaev, A simple model of quantum holography, talks at Kavli Institute for Theoretical Physics, Santa Barbara U.S.A. (2015).
[3] S. Sachdev, Phys. Rev. X **5**, 041025 (2015).
[4] J. Maldacena and D. Stanford, Phys. Rev. D **94**, 106002 (2016).
[5] S. Sachdev, Phys. Rev. Lett. **105**, 151602 (2010).
[6] J. Maldacena, S. H. Shenker, and D. Stanford, J. High Energy Phys. 08 (2016) 106.
[7] Y.-Z. You, A. W. W. Ludwig, and C. Xu, Phys. Rev. B **95**, 115150 (2017).
[8] J. Polchinski and V. Rosenhaus, J. High Energy Phys. 04 (2016) 001.
[9] A. M. García-García and J. J. M. Verbaarschot, Phys. Rev. D **94**, 126010 (2016).
[10] W. Fu, D. Gaiotto, J. Maldacena, and S. Sachdev, Phys. Rev. D **95**, 026009 (2017).
[11] S. Banerjee and E. Altman, Phys. Rev. B **95**, 134302 (2017).
[12] Y. Gu, X.-L. Qi, and D. Stanford, J. High Energy Phys. 05 (2017) 125.
[13] M. Berkooz, P. Narayan, M. Rozali, and J. Simón, J. High Energy Phys. 01 (2017) 138.
[14] P. Hosur, X.-L. Qi, D. A. Roberts, and B. Yoshida, J. High Energy Phys. 02 (2016) 004.
[15] C. Liu, X. Chen, and L. Balents, Phys. Rev. B **97**, 245126 (2018).
[16] Y. Huang and Y. Gu, arXiv:1709.09160.
[17] X.-Y. Song, C.-M. Jian, and L. Balents, Phys. Rev. Lett. **119**, 216601 (2017).
[18] Z. Bi, C.-M. Jian, Y.-Z. You, K. A. Pawlak, and C. Xu, Phys. Rev. B **95**, 205105 (2017).
[19] E. Lantagne-Hurtubise, C. Li, and M. Franz, Phys. Rev. B **97**, 235124 (2018).
[20] M. Franz and M. Rozali, Nat. Rev. Mater. **3**, 491 (2018).
[21] I. Danshita, M. Hanada, and M. Tezuka, Prog. Theor. Exp. Phys. **2017**, 083I01 (2017).
[22] D. I. Pikulin and M. Franz, Phys. Rev. X **7**, 031006 (2017).
[23] A. Chew, A. Essin, and J. Alicea, Phys. Rev. B **96**, 121119 (2017).

[24] A. Chen, R. Ilan, F. de Juan, D. I. Pikulin, and M. Franz, Phys. Rev. Lett. **121**, 036403 (2018).
[25] O. Parcollet, A. Georges, G. Kotliar, and A. Sengupta, Phys. Rev. B **58**, 3794 (1998).
[26] N. V. Gnezdilov, J. A. Hutasoit, and C. W. J. Beenakker, Phys. Rev. B **98**, 081413 (2018).
[27] I. Affleck and A. W. W. Ludwig, Nucl. Phys. B **360**, 641 (1991).
[28] Y. Meir and N. S. S. Wingreen, Phys. Rev. Lett. **68**, 2512 (1992).
[29] G. D. Mahan, *Many-Particle Systems* (Plenum, New York, 2000).
[30] S. Sachdev, *Quantum Phase Transitions* (Cambridge University Press, Cambridge, 2001).
[31] A. C. Hewson, *The Kondo Problem to Heavy Fermions* (Cambridge University Press, Cambridge, 1993).
[32] H. J. W. Haug and A.-P. Jauho, *Quantum Kinetics in Transport and Optics of Semiconductors* (Springer, Berlin, 2008).
[33] I. Affleck and A. W. W. Ludwig, Phys. Rev. B **48**, 7297 (1993).
[34] D. C. Ralph, A. W. W. Ludwig, J. von Delft, and R. A. Buhrman, Phys. Rev. Lett. **72**, 1064 (1994).
[35] J. v. Delft, A. W. W. Ludwig, and V. Ambegaokar, Ann. Phys. (NY) **273**, 175 (1999).
[36] M. H. Hettler, J. Kroha, and S. Hershfield, Phys. Rev. Lett. **73**, 1967 (1994).
[37] M. H. Hettler, J. Kroha, and S. Hershfield, Phys. Rev. B **58**, 5649 (1998).
[38] R. M. Potok, I. G. Rau, H. Shtrikman, Y. Oreg, and D. Goldhaber-Gordon, Nature (London) **446**, 167 (2007).
[39] U. Weiss, *Quantum Dissipative Systems* (World Scientific, Singapore, 2008).
[40] J. W. Negele and H. Orland, *Quantum Many-Particle Systems* (Westview, Boulder, CO, 1998), p. 51.
[41] O. Parcollet and A. Georges, Phys. Rev. B **59**, 5341 (1999).
[42] I. S. Gradshteyn and I. M. Ryzhik, in *Table of Integrals, Series, and Products*, edited by A. Jeffrey and D. Zwilinger (Academic, New York, 2000).
[43] *Handbook of Mathematical Functions*, edited by M. Abramowitz and I. A. Stegun (National Bureau of Standards, Gaithersburg, MD, 1972).
[44] J. Rammer and H. Smith, Rev. Mod. Phys. **58**, 323 (1986).
[45] A. Kamenev, in *Nanophysics: Coherence and Transport*, Vol. 81, edited by H. Bouchiat, Y. Gefen, S. Guéron, G. Montambaux, and J. Dalibard, Lecture Notes of the Les Houches Summer School (Elsevier, Amsterdam, 2004), p. 177.
[46] J. Vanderplas, Non-equispaced fast Fourier transform for Python (2018), https://github.com/jakevdp/nfft.
[47] D. C. Langreth, in *Linear and Nonlinear Electron Transport in Solids*, 8, Vol. 17, edited by J. T. Devreese and E. van Doren, NATO Advanced Study Institute (Springer, New York, 1976), p. 9.
[48] N. S. Wingreen and Y. Meir, Phys. Rev. B **49**, 11040 (1994).
[49] S. Hershfield, J. H. Davies, and J. W. Wilkins, Phys. Rev. B **46**, 7046 (1992).
[50] L. P. Kadanoff and G. Baym, *Quantum Statistical Mechanics* (W. A. Benjamin, New York, 1962).
[51] T. Giamarchi, *Quantum Physics in One Dimension* (Clarendon, Oxford, 2003), p. 306.